Supplementary Information (SI) for New Journal of Chemistry.

SUPPORT INFORMATION

Quinoxaline Derivatives as Potent Compounds against Both 3CL^{pro} and PL^{pro} Enzymes of SARS-CoV-2 virus: An Insight from Experimental and Theoretical Approaches.

Nazanin Noroozi-Shad [1], Hossein Sabet-Sarvestani [1], Vahid Moghimi [2], Toktam Afrough [1], Kamahldin Haghbeen [3]*, Hossein Eshghi [1]*

[1] *Department of Chemistry, Faculty of Science, Ferdowsi University of Mashhad, Mashhad, Iran.*
[2] *Department of Biology, Faculty of Science, Hakim Sabzevari University, Sabzevar, Iran.*
[3] *Department of Plant Bioproducts, National Institute of Genetic Engineering and Biotechnology, Tehran, Iran.*

*Corresponding authors: H. Eshghi (heshghi@um.ac.ir, Phone: +98 9155246703) and K. Haghbeen (kamahl@nigeb.ac.ir, phone: +98 21 44787372, P.O.Box: 14965/161, Tehran, Iran)

Molecular Dynamics Simulation

AMBER99SB-ILDN force field implanted in Gromacs2020 was used for the simulation of the final models. The docked complex was solvated in a cubic box with simple point charge (SPC) waters, and Na^+ or Cl^- counter ions were added to the system for the overall electrostatic neutrality. The Particle Mesh Ewald (PME) method was used to evaluate the Long-range electrostatic interactions, in which the cutoff distance was considered 1.2 Å for the long-range Van der Waals (VDW) energy. Also using V-rescale, the temperature was readjusted during the simulation time. First, energy minimization of the whole system was performed without any restraints for 50,000 iteration steps using the steepest descent algorithm. Afterward, the systems were equilibrated through two separated simulation steps. At the first step, the equilibrium state of the system was reached via a constant number of particles, volume, and temperature (NVT ensemble protocol) for 200 ps simulation at 300 K, in which the Verlet scheme was utilized to control the temperature. By the same simulation time, the second phase of equilibration was performed using a constant number of particles, pressure, and temperature (NPT ensemble protocol) at 300 K, in which Verlet scheme and Berendsen barostat were applied to control temperature and pressure (constant to 1 Bar), respectively. LINCS algorithm was used to covalent bond restrictions in the equilibration steps. The ultimate production step was performed for 50 ns of MD simulation under a constant temperature of 300 K, in which trajectories were saved every 1 fs.

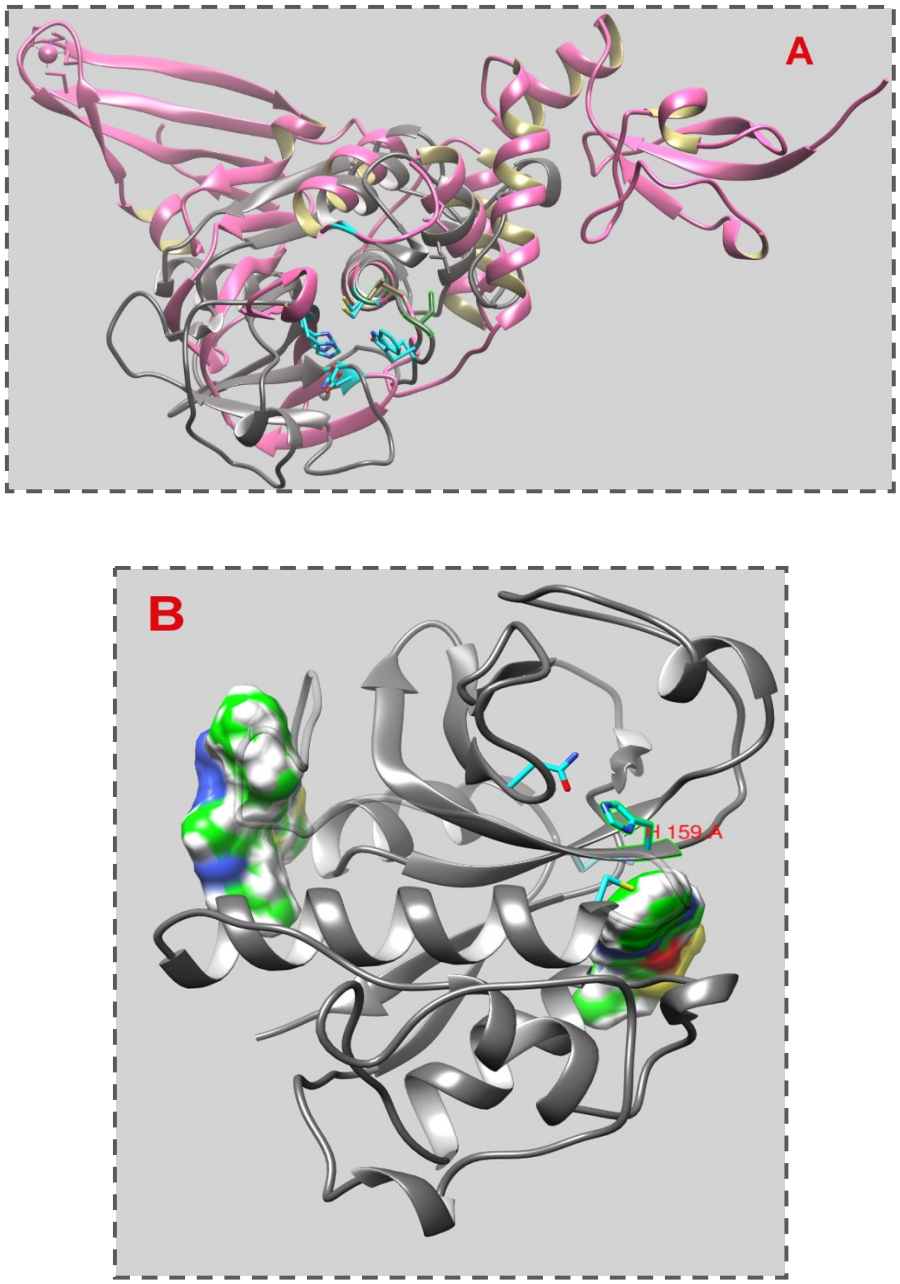

FIGURE S1 A) The overlaid structures of papain (PDB: 1PPN; in brown color) with PL^{pro} (PDB: 2FE8; in pink color). B) Illustration of 2 cavities in 1PPN including the active site pocket and a non-specific binding site.

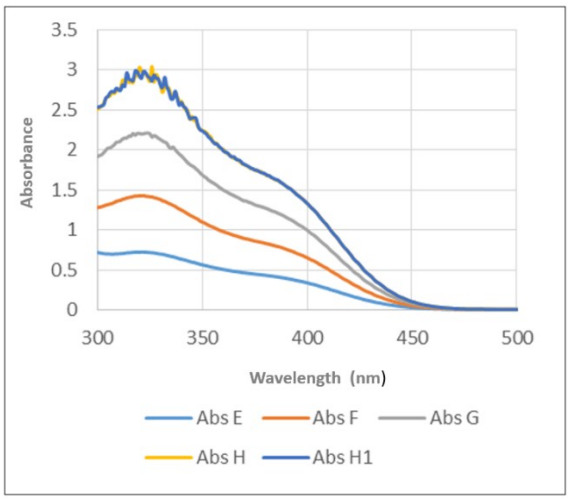

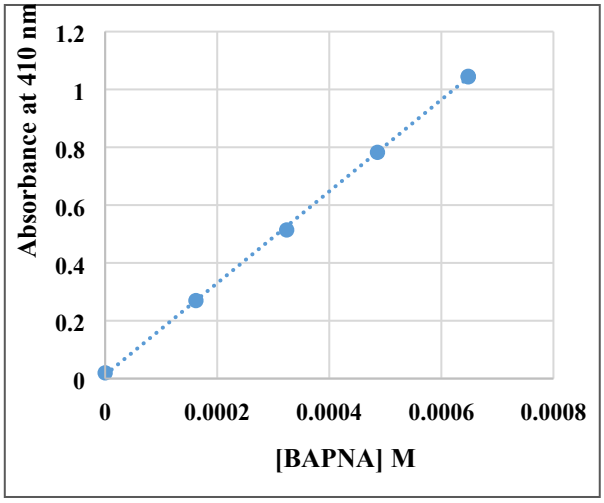

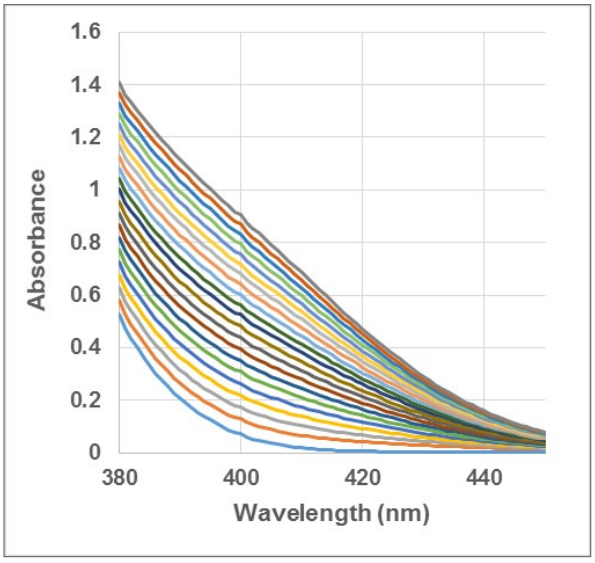

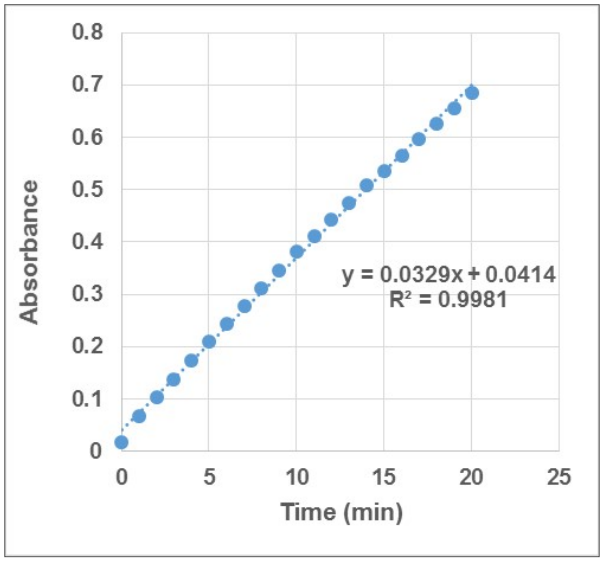

FIGURE S2 Spectrophotometric follow-up of papain (1.2 mg mL^{-1}) reactions **TOP)** at different concentrations and **DOWN)** at a constant concentration of BAPNA (0.56 mM) using wavelength scans at the end of the reactions (Top) and during the progress of a reaction (Down), respectively. Reactions were carried out in Tris buffer (0.05 M, pH 7.5) at 30 ℃.

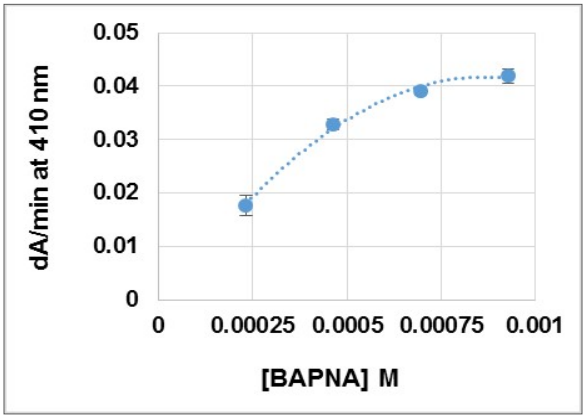

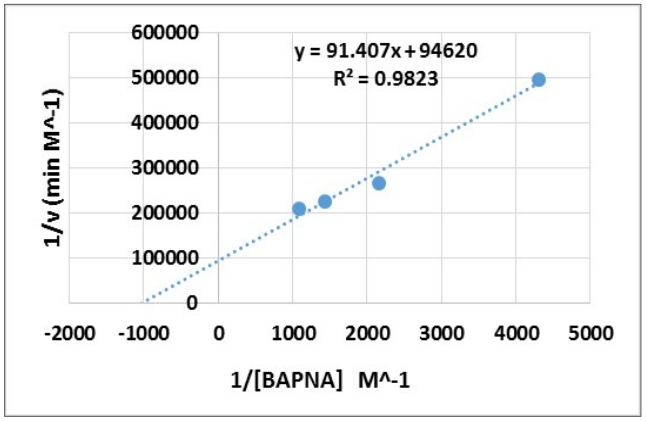

V_{max} = 1.06 x 10^{-5} M min^{-1} K_m = 9.66 x 10^{-4} M

FIGURE S3 Kinetics curve of BAPNA in the presence of papain (left) and Lineweaver-Burk plot (right) of the kinetics curve (See the experimental section for the details.)

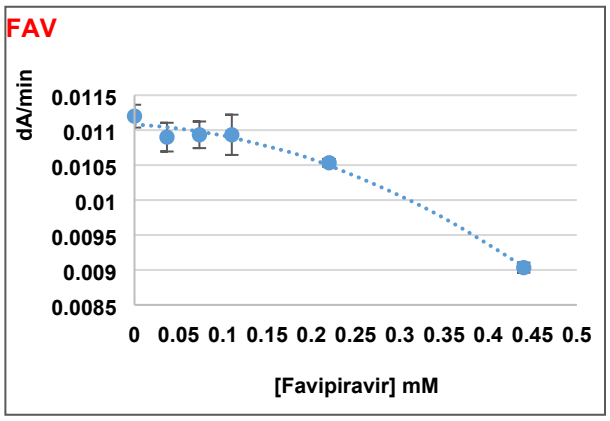

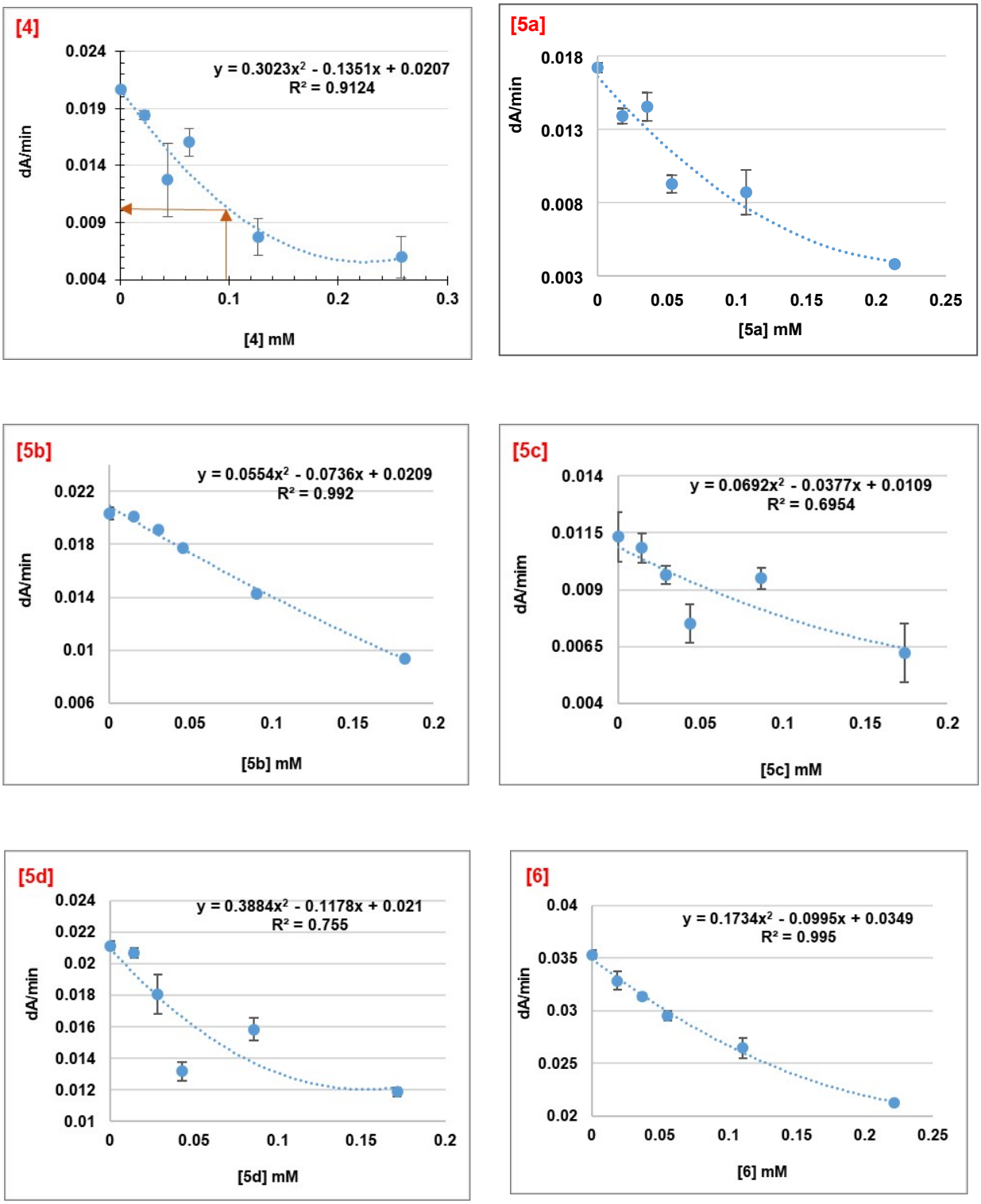

FIGURE S4 Inhibition kinetics curves of papain reactions with BAPNA in the presence of various concentrations of Favipiravir (FAV) and the quinoxaline derivatives (**4**, **5a-d**, and **6**).

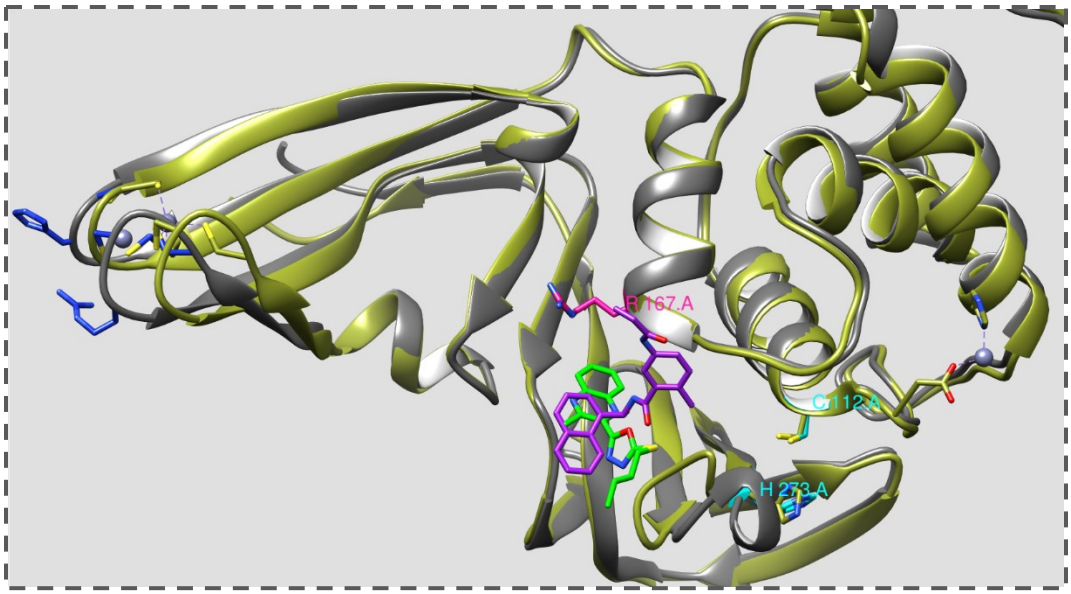

FIGURE S5 Overlaid structures of the complexes of **5a-2FE8** and wild PLpro-PLP-Synder350. PLP-Synder350 and **5a** are in purple and green, respectively.

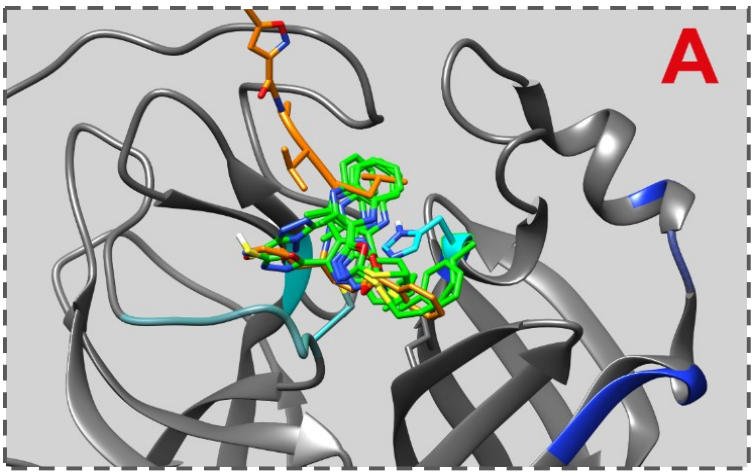

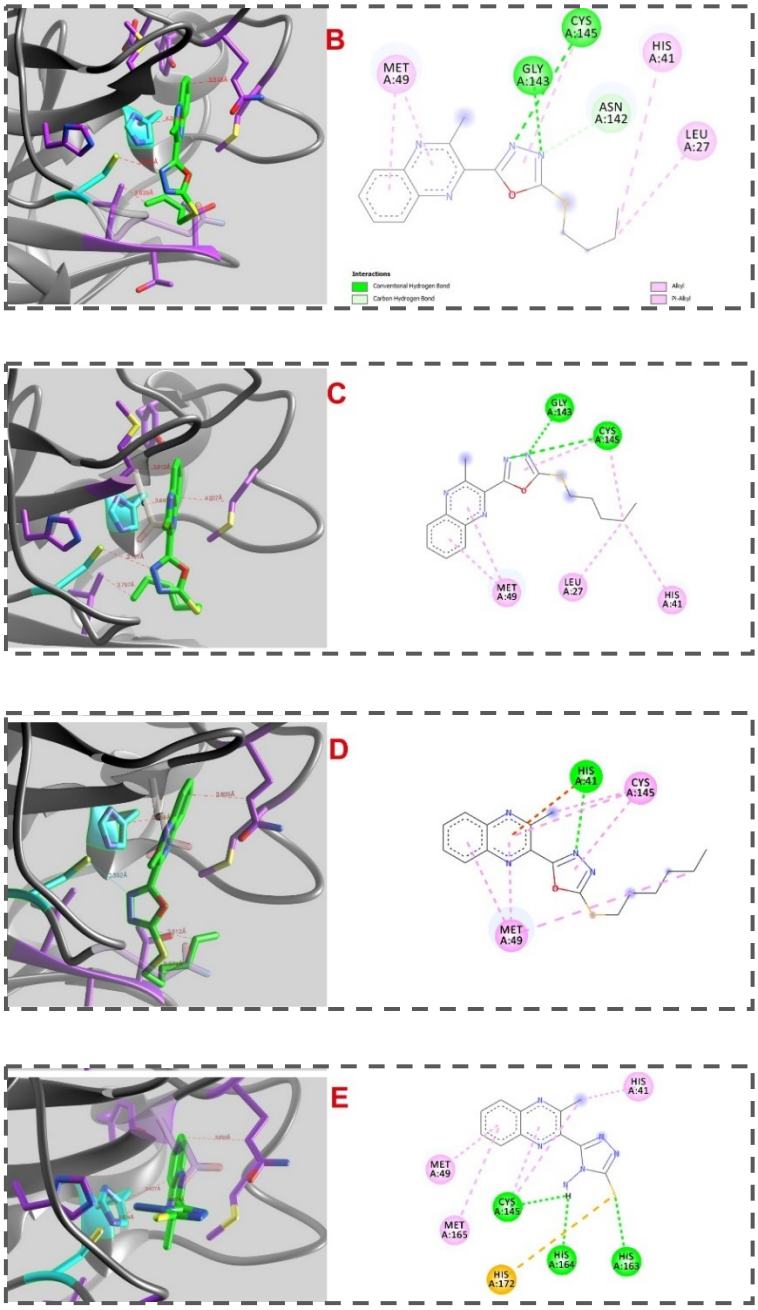

FIGURE S6 A) The overlaid poses of the synthesized quinoxaline derivatives with the crystallographic report of the complex of N3 and $3CL^{pro}$ (PDB: 6LU7). The most favorable binding poses of B) **5a**, C) **5b**, D) **5c**, and E) **6** in $3CL^{pro}$. H41 (Histidine41) and C145 (Cysteine145) are in turquoise color. The neighboring residues to each ligand at distances ≤4.5 Å are illustrated.

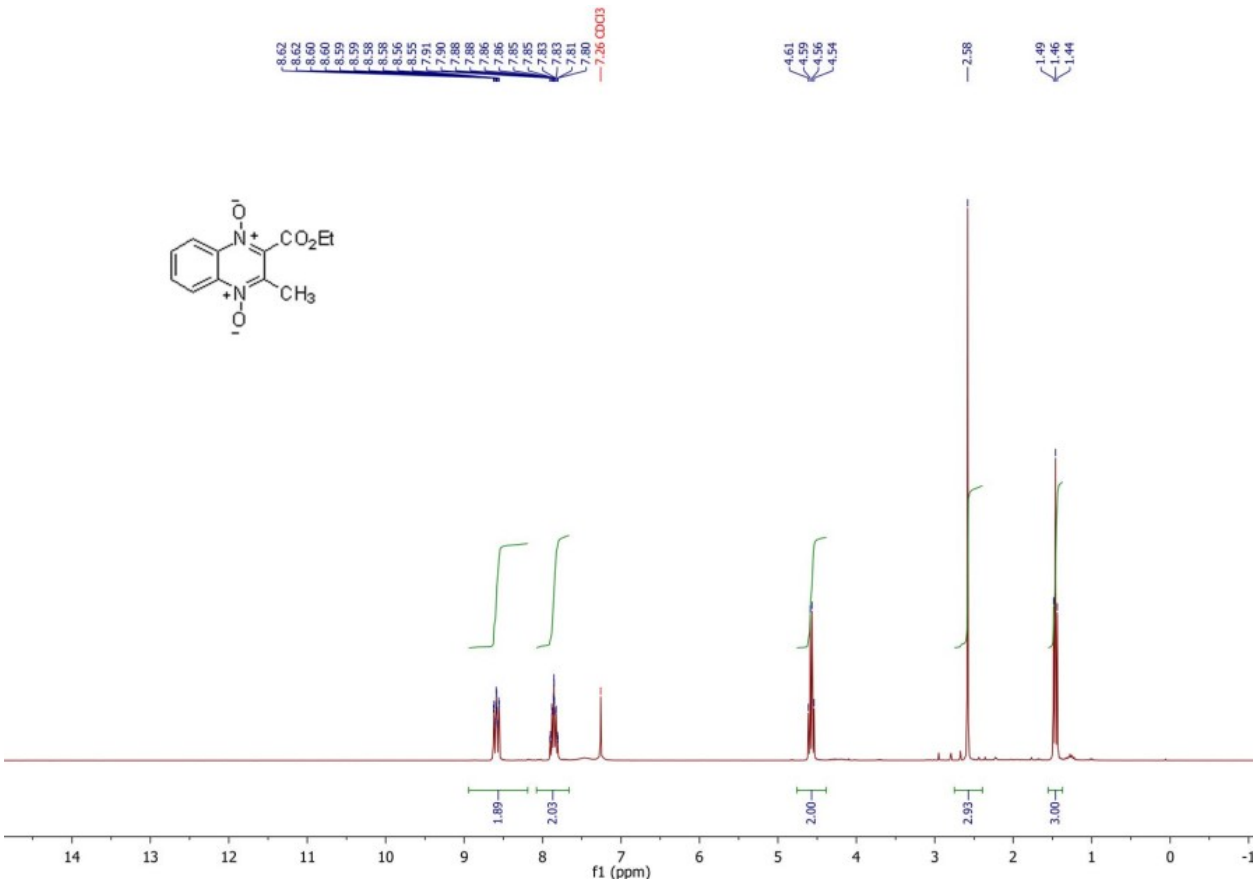

FIGURE S7 ^{1}H NMR (300 MHz, $CDCl_3$) of 2-(ethoxycarbonyl)-3-methylquinoxaline 1,4-dioxide (**2**)

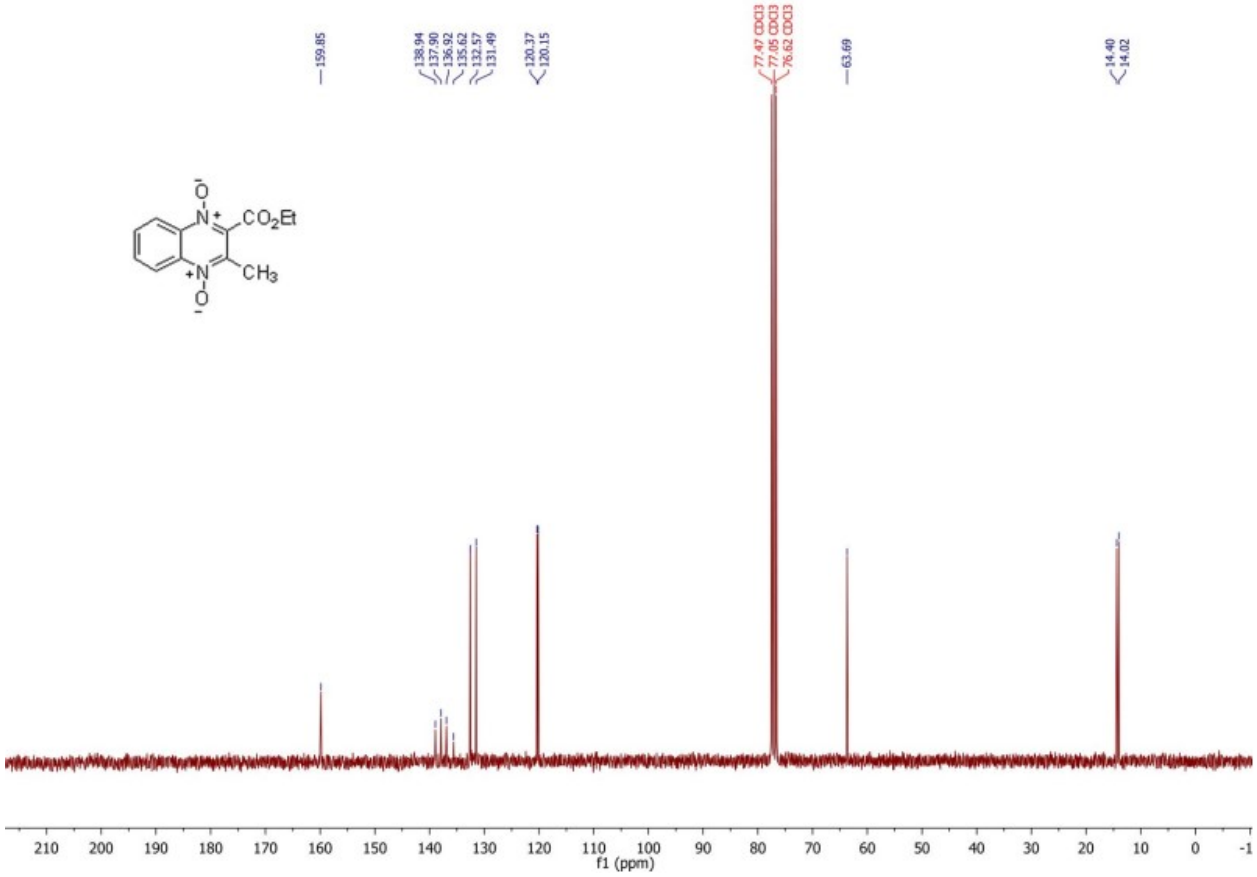

FIGURE S8 ^{13}C NMR (75 MHz, $CDCl_3$) of 2-(ethoxycarbonyl)-3-methylquinoxaline 1,4-dioxide (**2**)

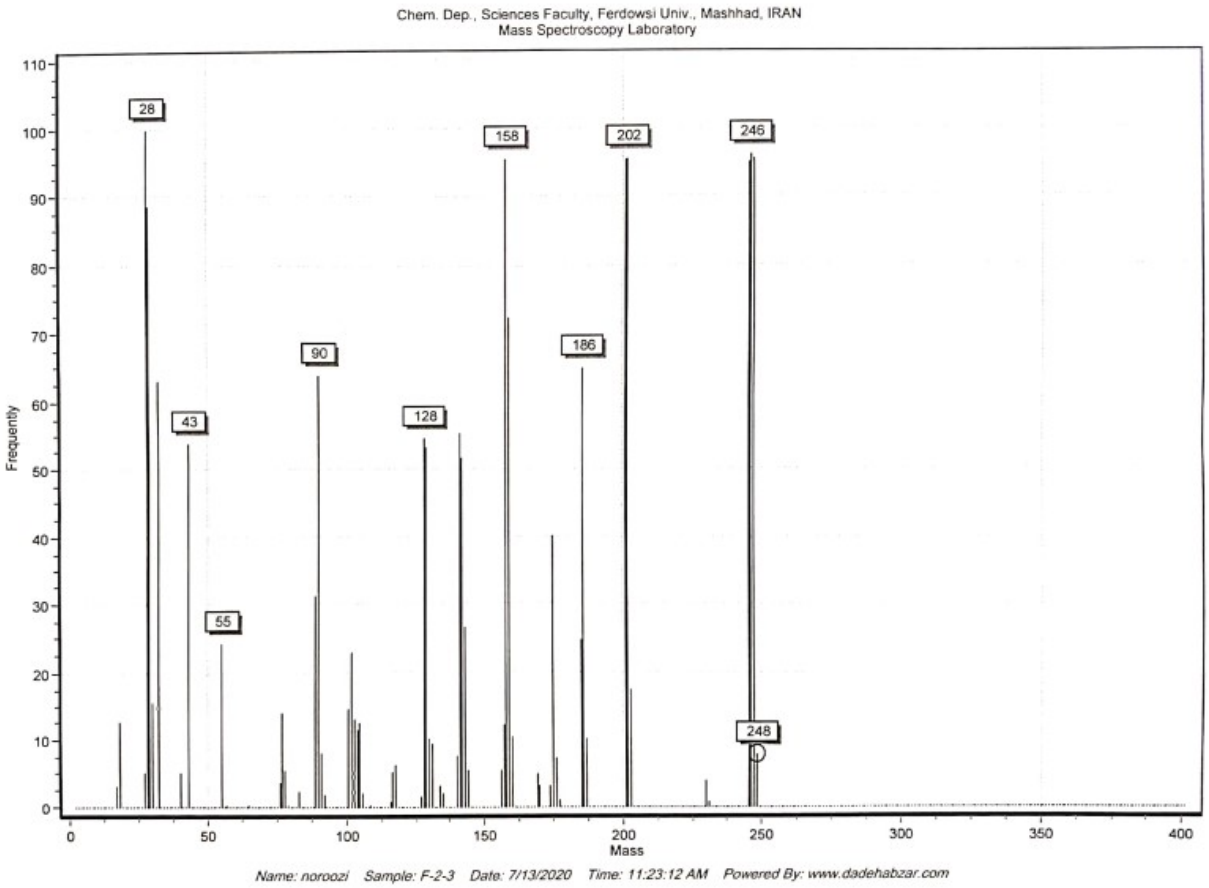

FIGURE S9 Mass spectrum of 2-(ethoxycarbonyl)-3-methylquinoxaline 1,4-dioxide (**2**)

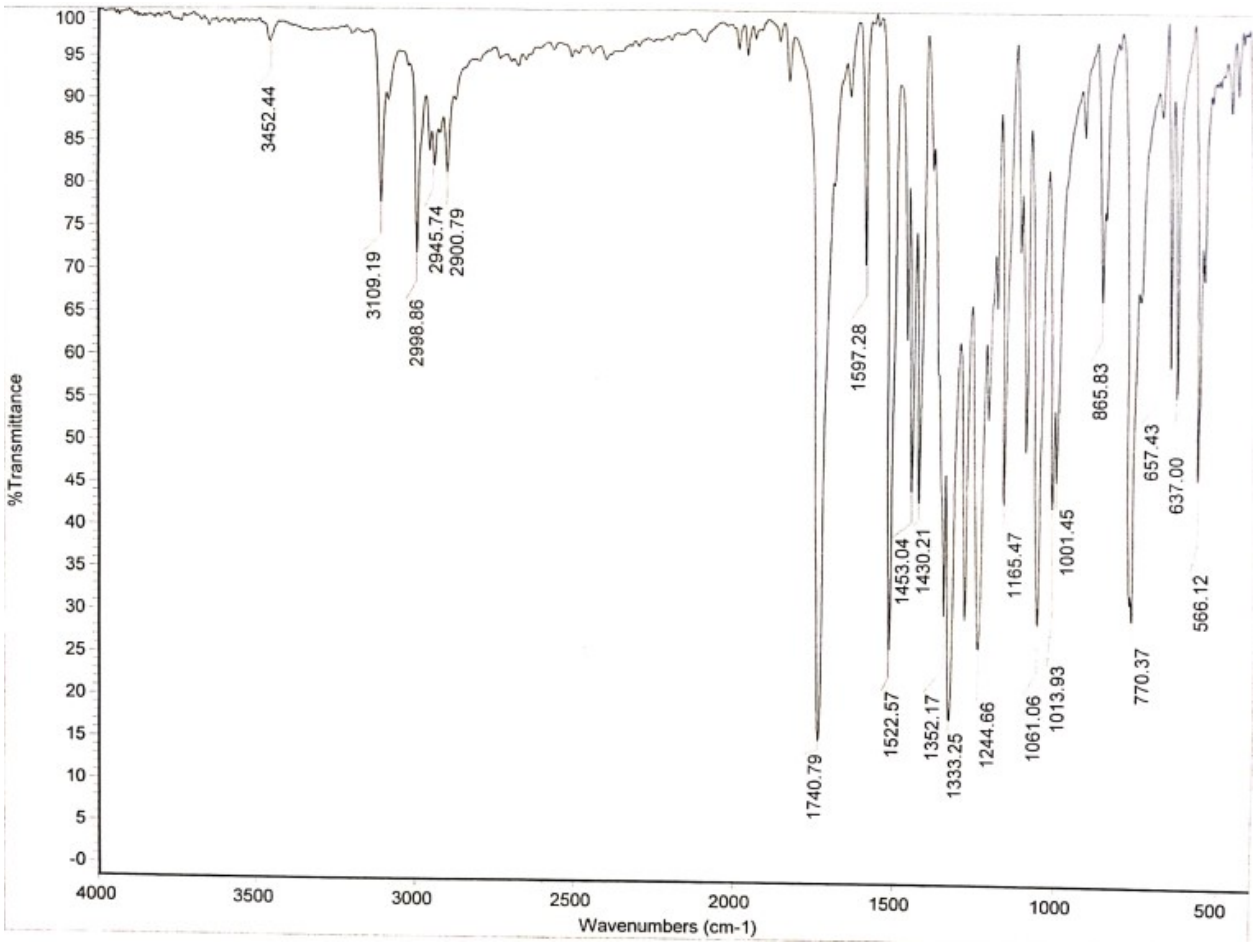

FIGURE S10 FT-IR (KBr) of 2-(ethoxycarbonyl)-3-methylquinoxaline 1,4-dioxide (**2**)

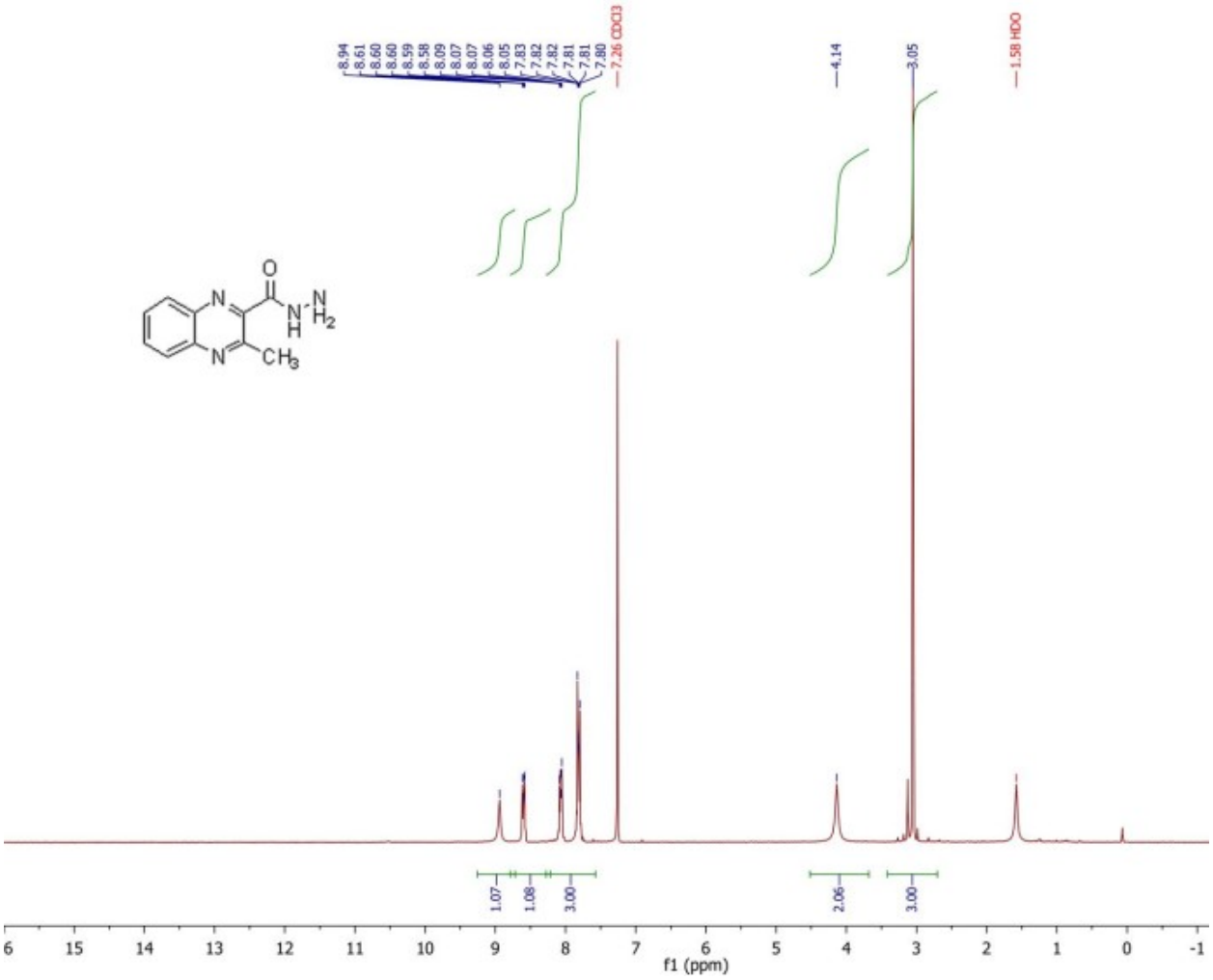

FIGURE S11 ^{1}H NMR (300 MHz, $CDCl_3$) of 3-methylquinoxaline-2-carbohydrazide (**3**)

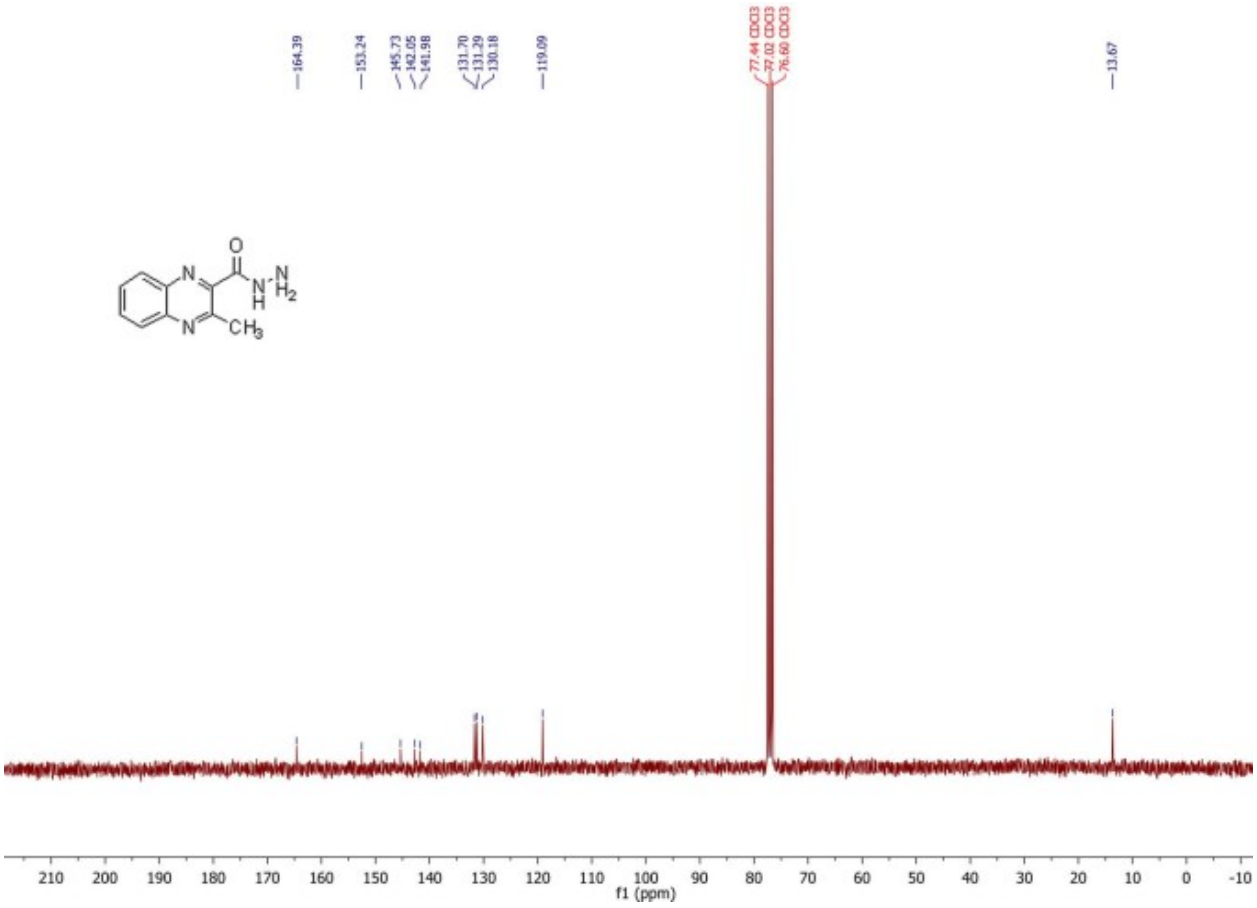

FIGURE S12 ^{13}C NMR (75 MHz, $CDCl_3$) of 3-methylquinoxaline-2-carbohydrazide (**3**)

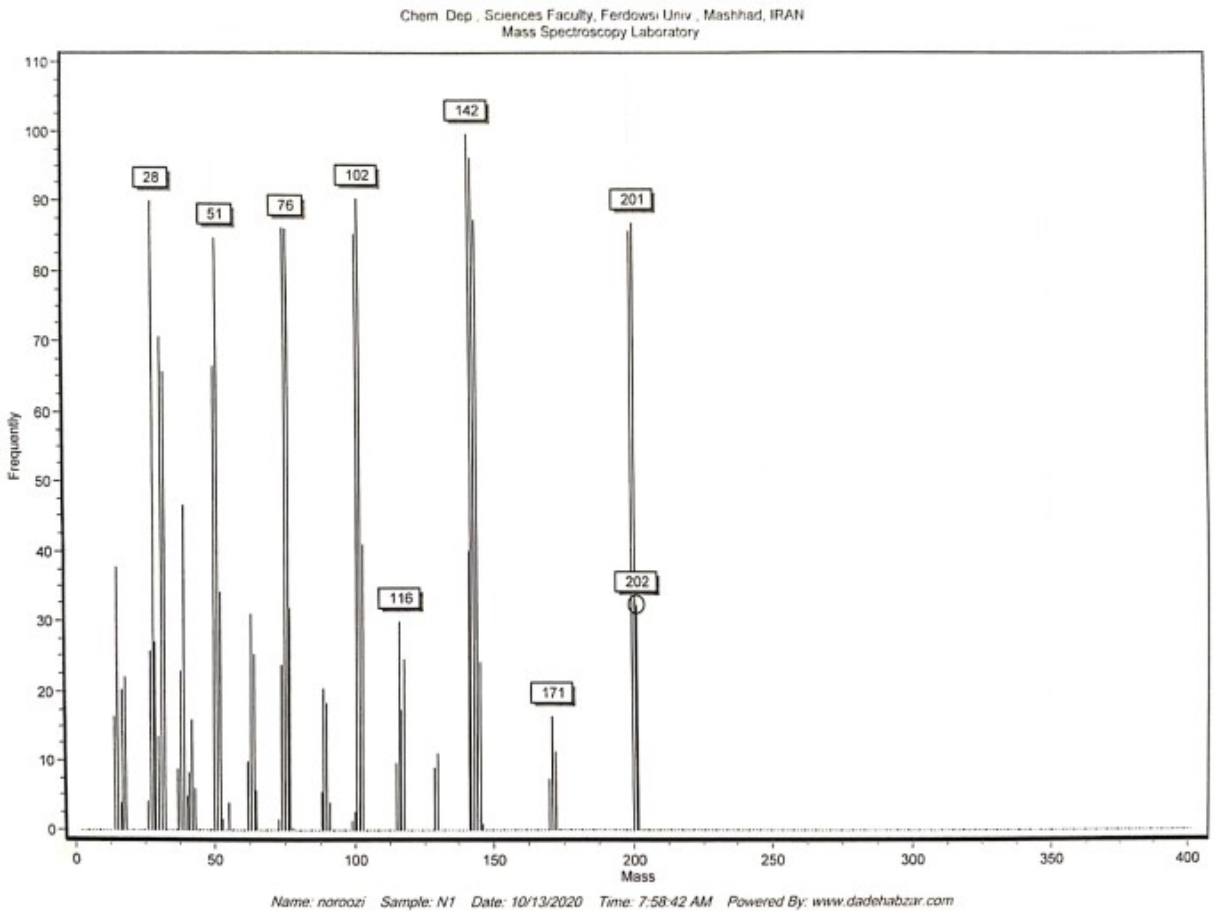

FIGURE S13 Mass spectrum of 3-methylquinoxaline-2-carbohydrazide (**3**)

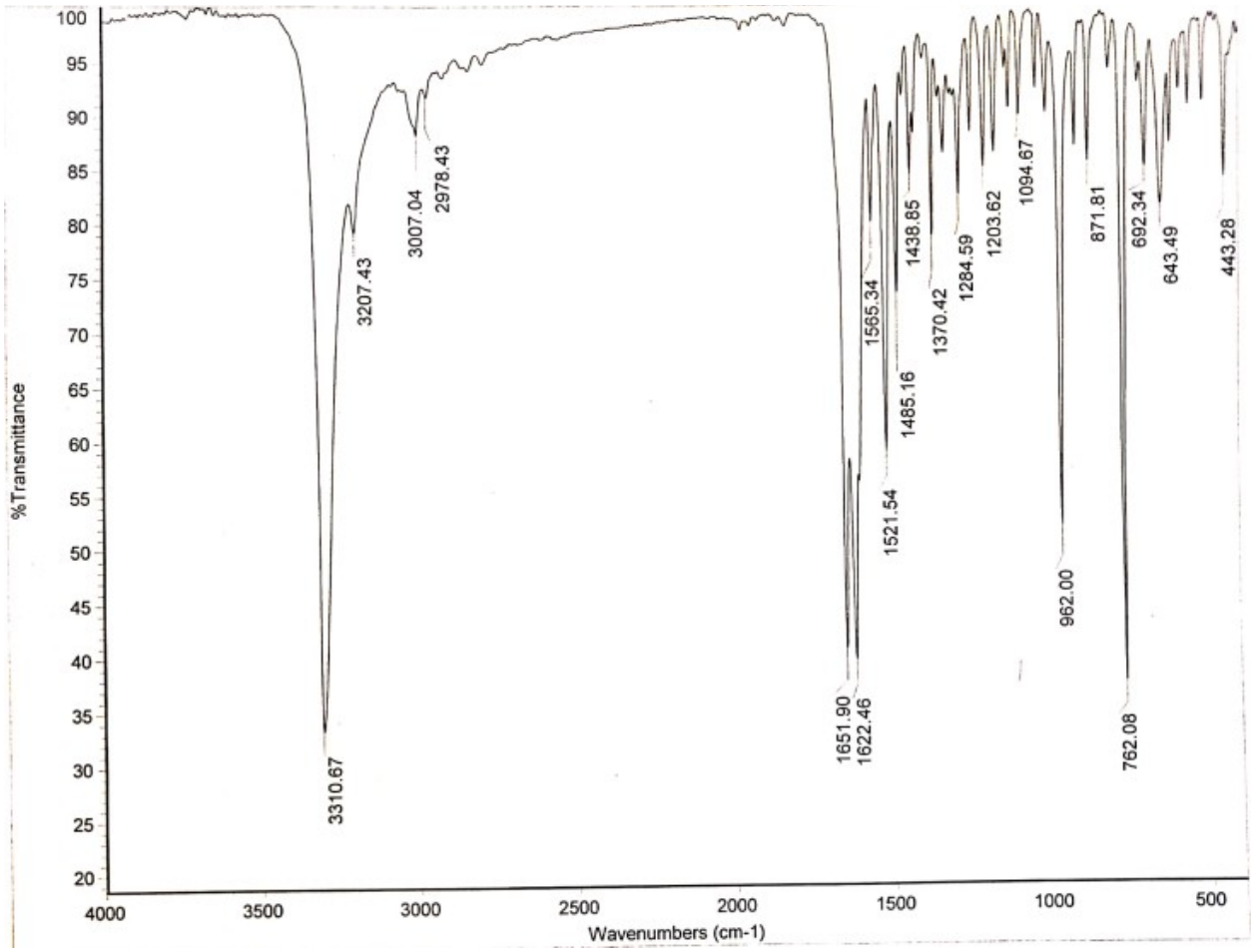

FIGURE S14 FT-IR (KBr) of 3-methylquinoxaline-2-carbohydrazide (**3**)

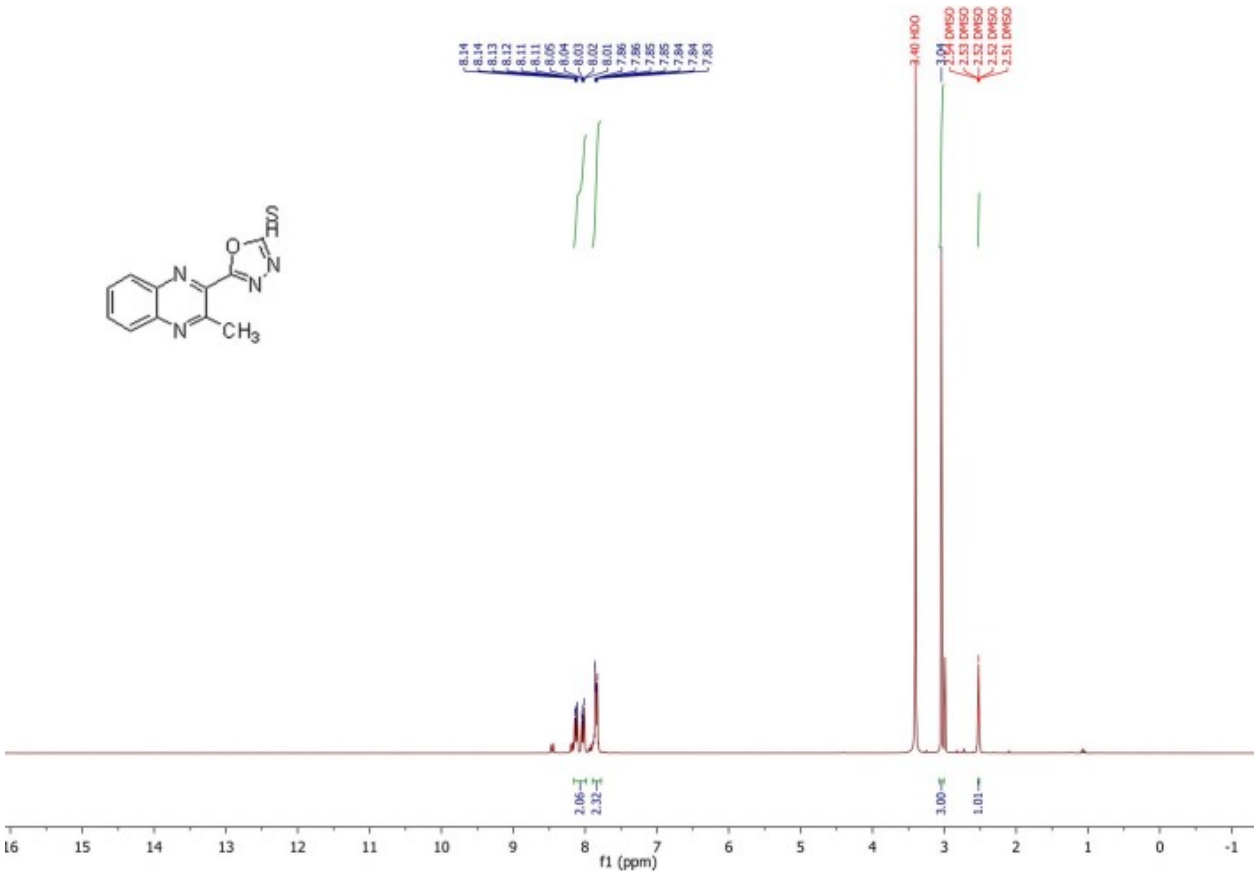

FIGURE S15 ^{1}H NMR (300 MHz, DMSO-d_6) 5-(3-methylquinoxalin-2-yl)-1,3,4-oxadiazole-2-thiol **(4)**

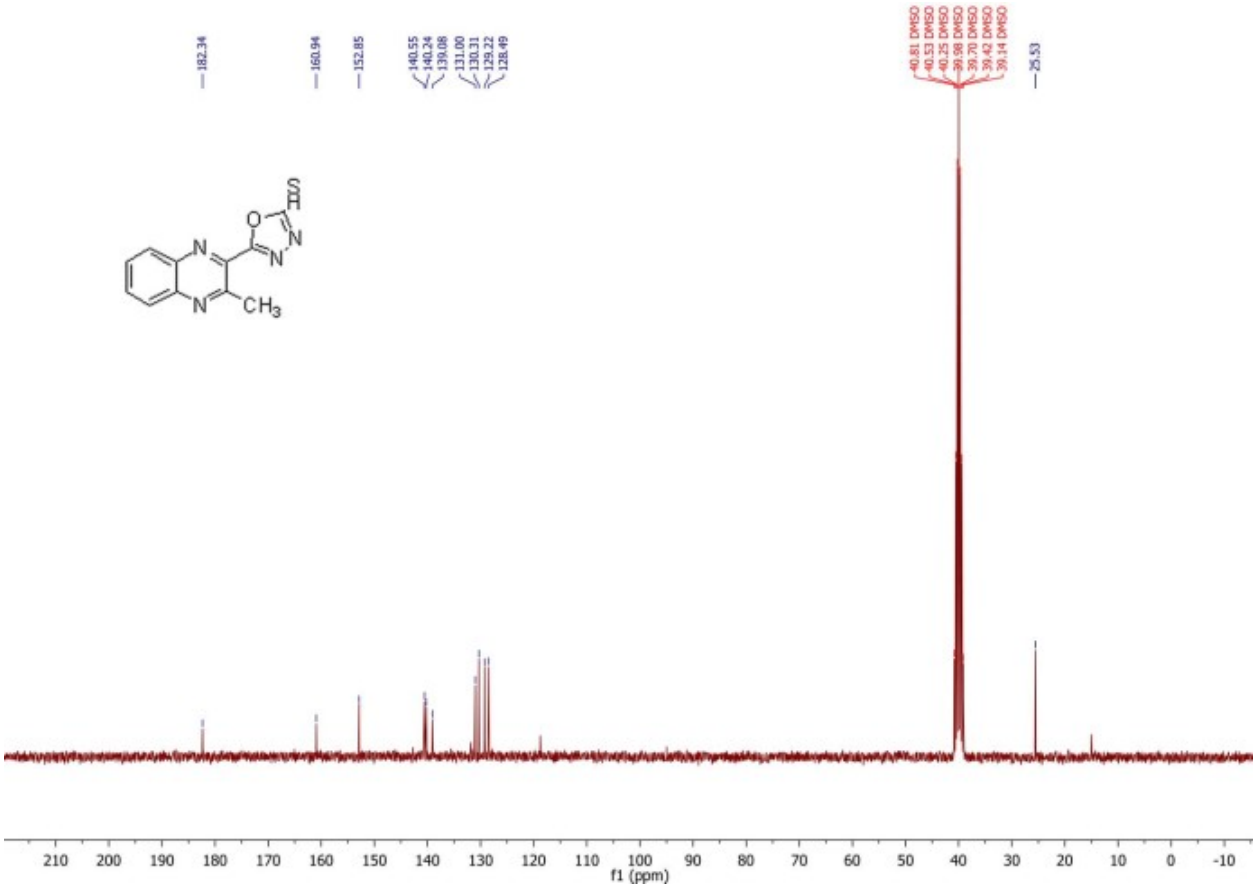

FIGURE S16 ^{13}C NMR (75 MHz, DMSO-d_6) of 5-(3-methylquinoxalin-2-yl)-1,3,4-oxadiazole-2-thiol **(4)**

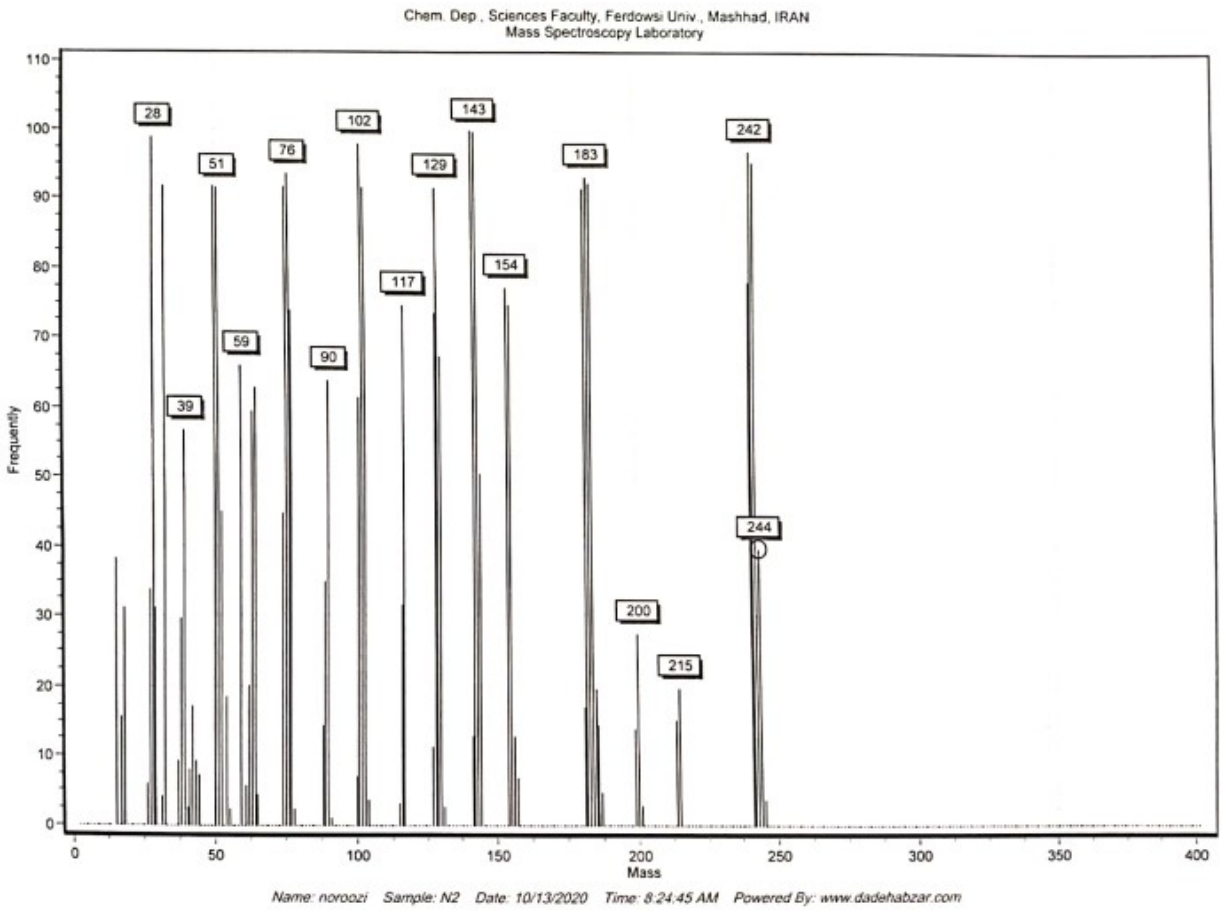

FIGURE S17 Mass spectrum of 5-(3-methylquinoxalin-2-yl)-1,3,4-oxadiazole-2-thiol **(4)**

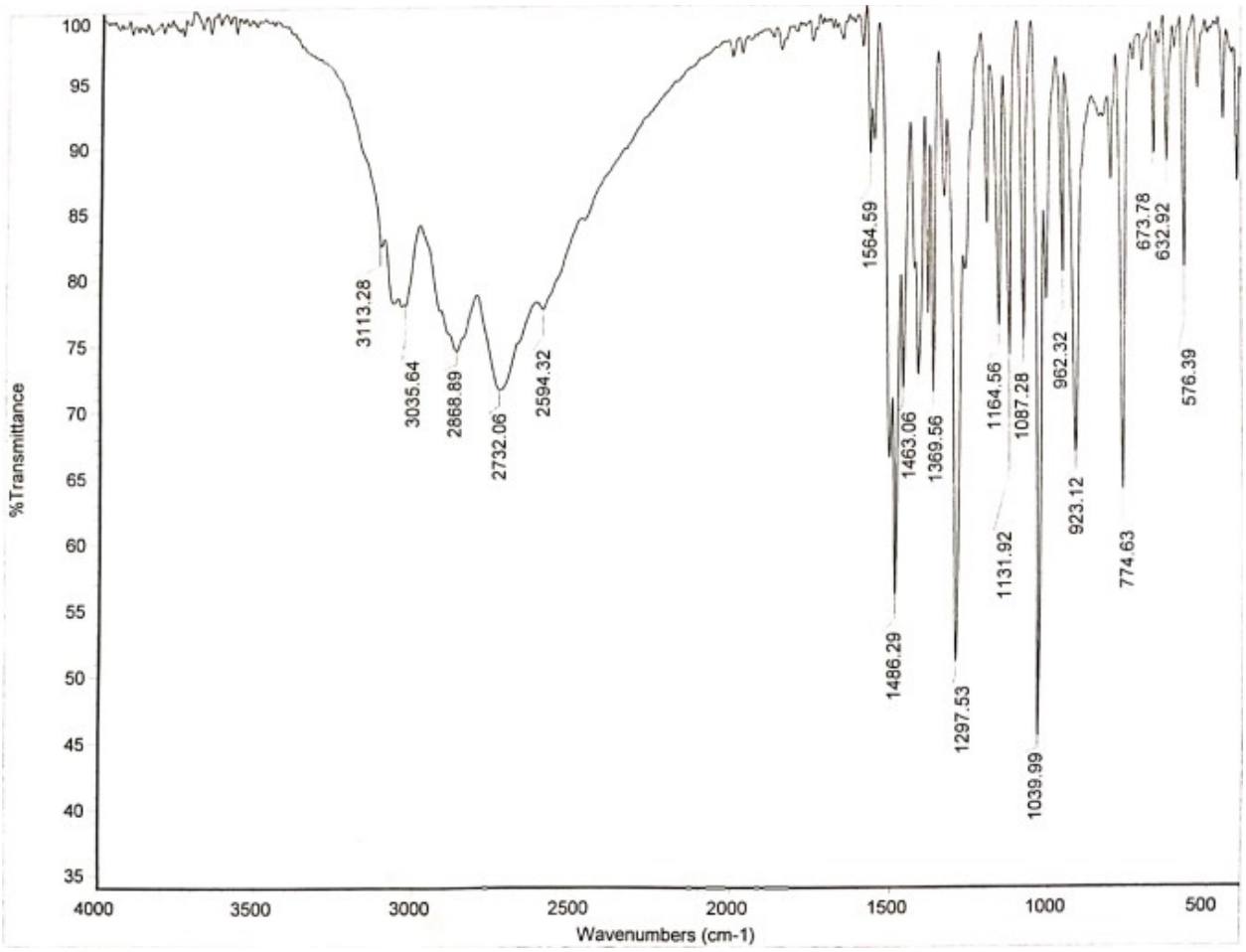

FIGURE S18 FT-IR (KBr) of 5-(3-methylquinoxalin-2-yl)-1,3,4-oxadiazole-2-thiol **(4)**

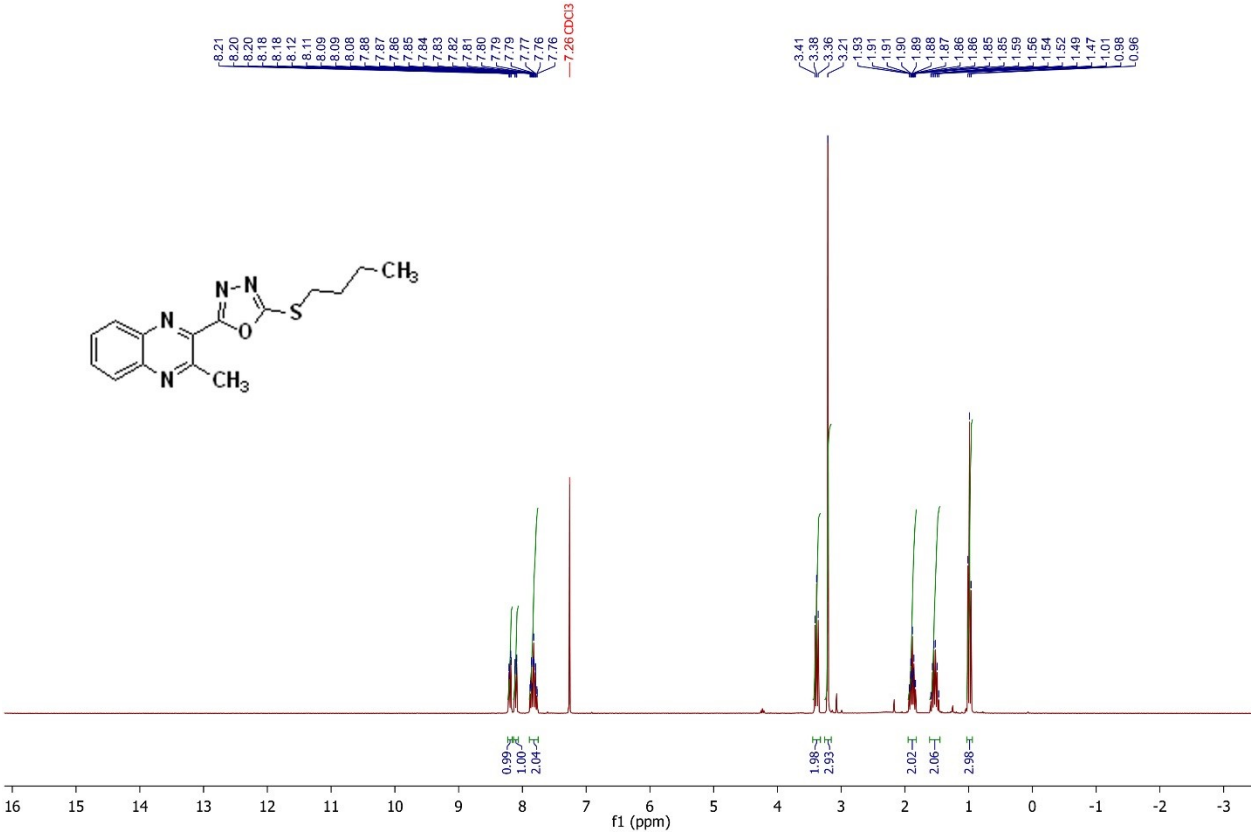

FIGURE S19 ^{1}H NMR (300 MHz, $CDCl_3$) of 2-(butylthio)-5-(3-methylquinoxalin-2-yl)-1,3,4-oxadiazole (**5a**)

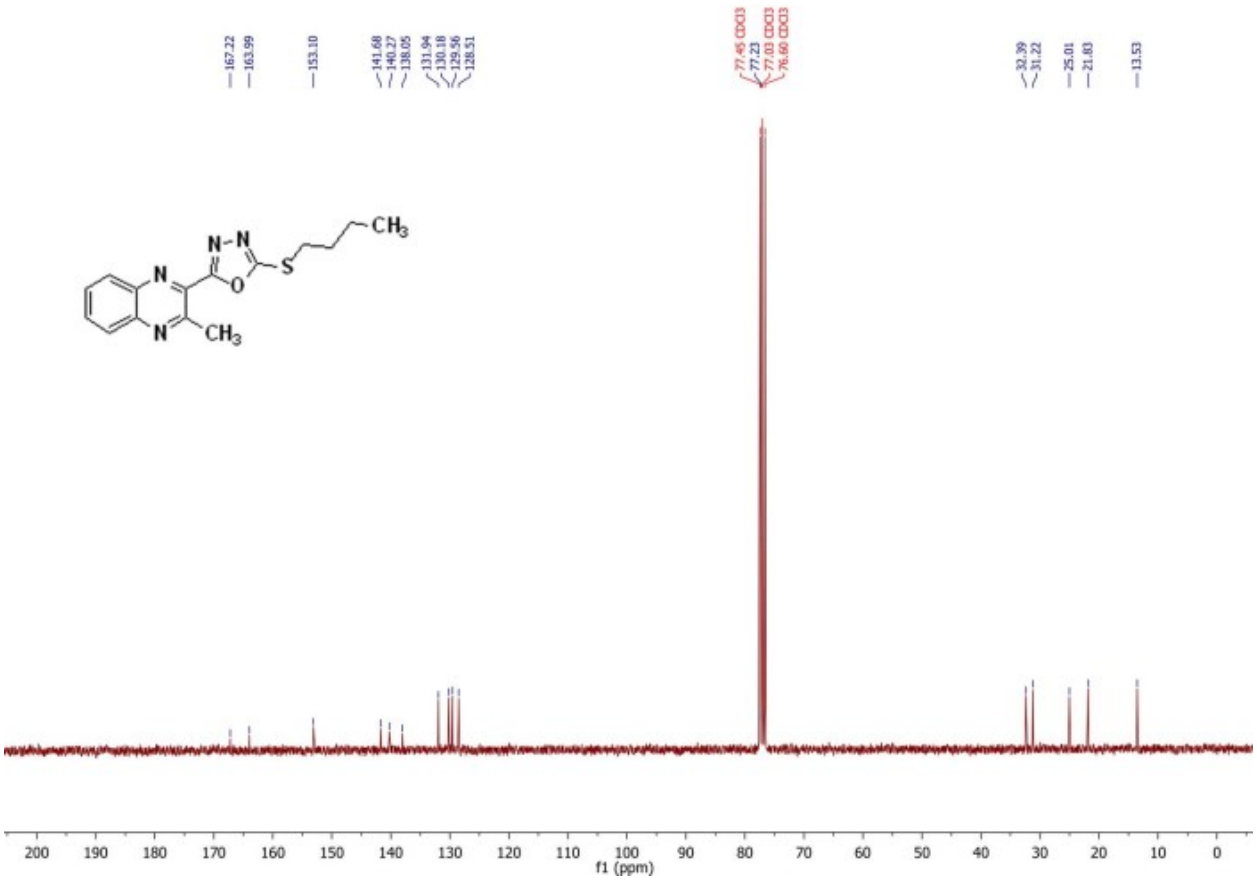

FIGURE S20 ^{13}C NMR (75 MHz, $CDCl_3$) of 2-(butylthio)-5-(3-methylquinoxalin-2-yl)-1,3,4-oxadiazole (**5a**)

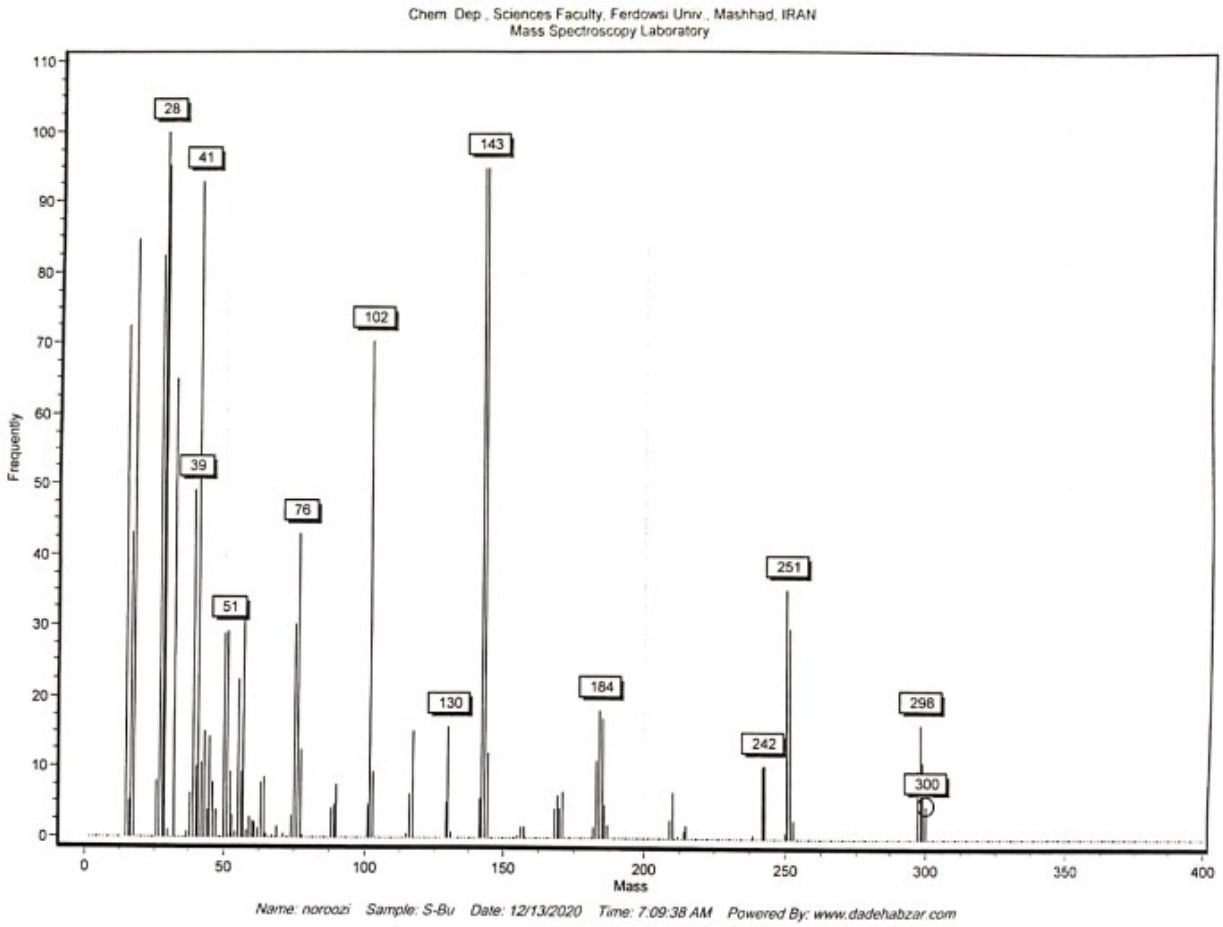

FIGURE S21 Mass spectrum of 2-(butylthio)-5-(3-methylquinoxalin-2-yl)-1,3,4-oxadiazole (**5a**)

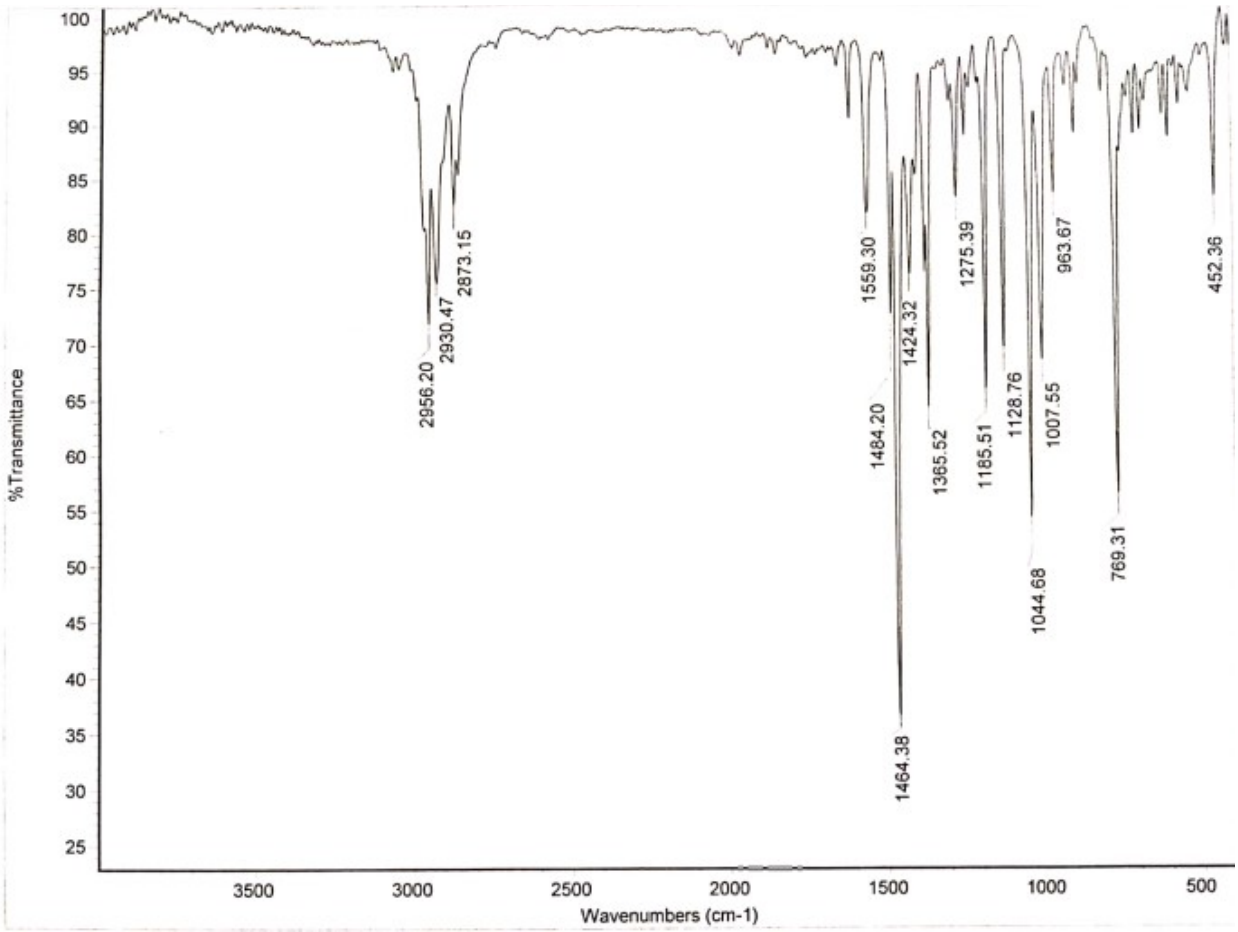

FIGURE S22 FT-IR (KBr) of 2-(butylthio)-5-(3-methylquinoxalin-2-yl)-1,3,4-oxadiazole (**5a**)

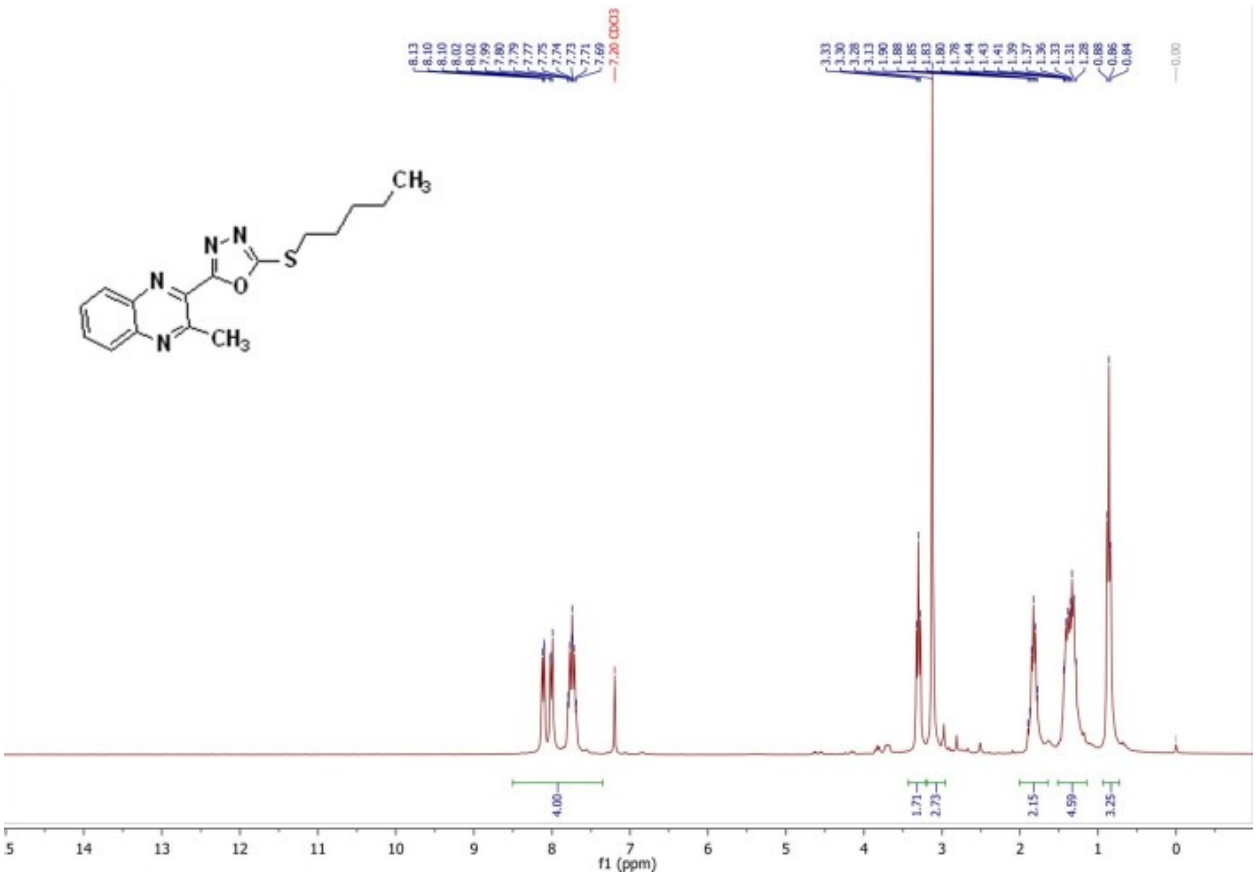

FIGURE S23 ^{1}H NMR (300 MHz, $CDCl_3$) of 2-(3-methylquinoxalin-2-yl)-5-(pentylthio)-1,3,4-oxadiazole (**5b**)

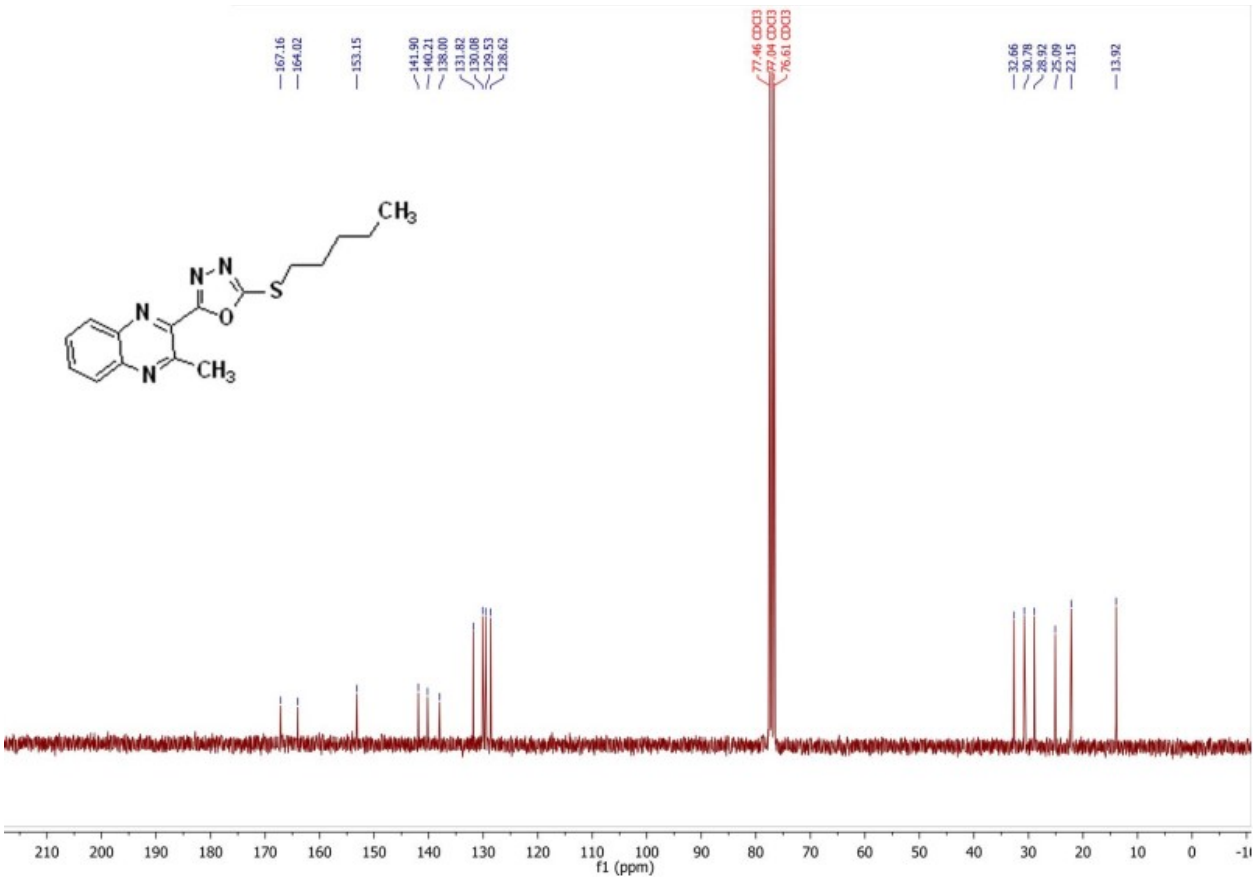

FIGURE S24 ^{13}C NMR (75 MHz, $CDCl_3$) of 2-(3-methylquinoxalin-2-yl)-5-(pentylthio)-1,3,4-oxadiazole (**5b**)

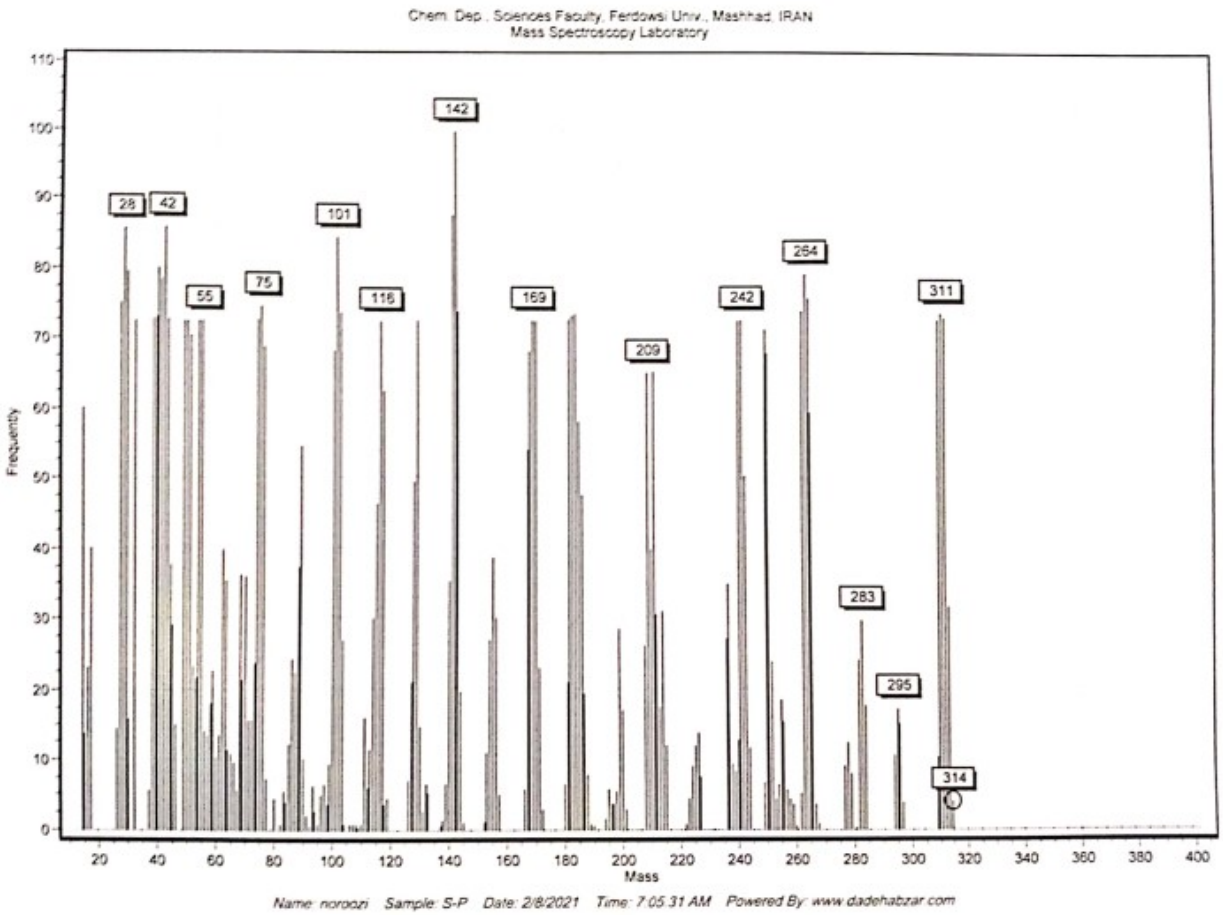

FIGURE S25 Mass spectrum of 2-(3-methylquinoxalin-2-yl)-5-(pentylthio)-1,3,4-oxadiazole (**5b**)

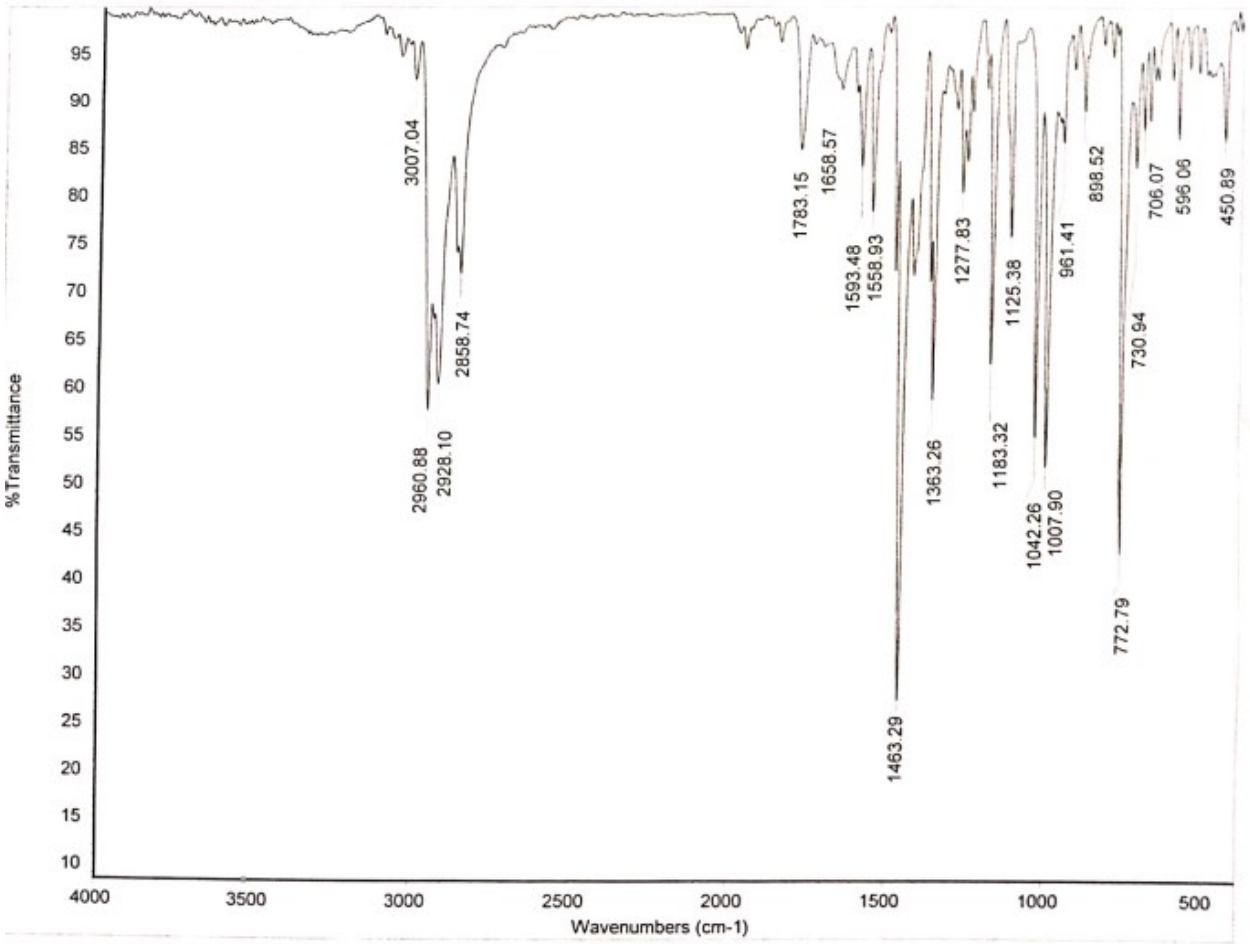

FIGURE S26 FT-IR (KBr) of 2-(3-methylquinoxalin-2-yl)-5-(pentylthio)-1,3,4-oxadiazole (**5b**)

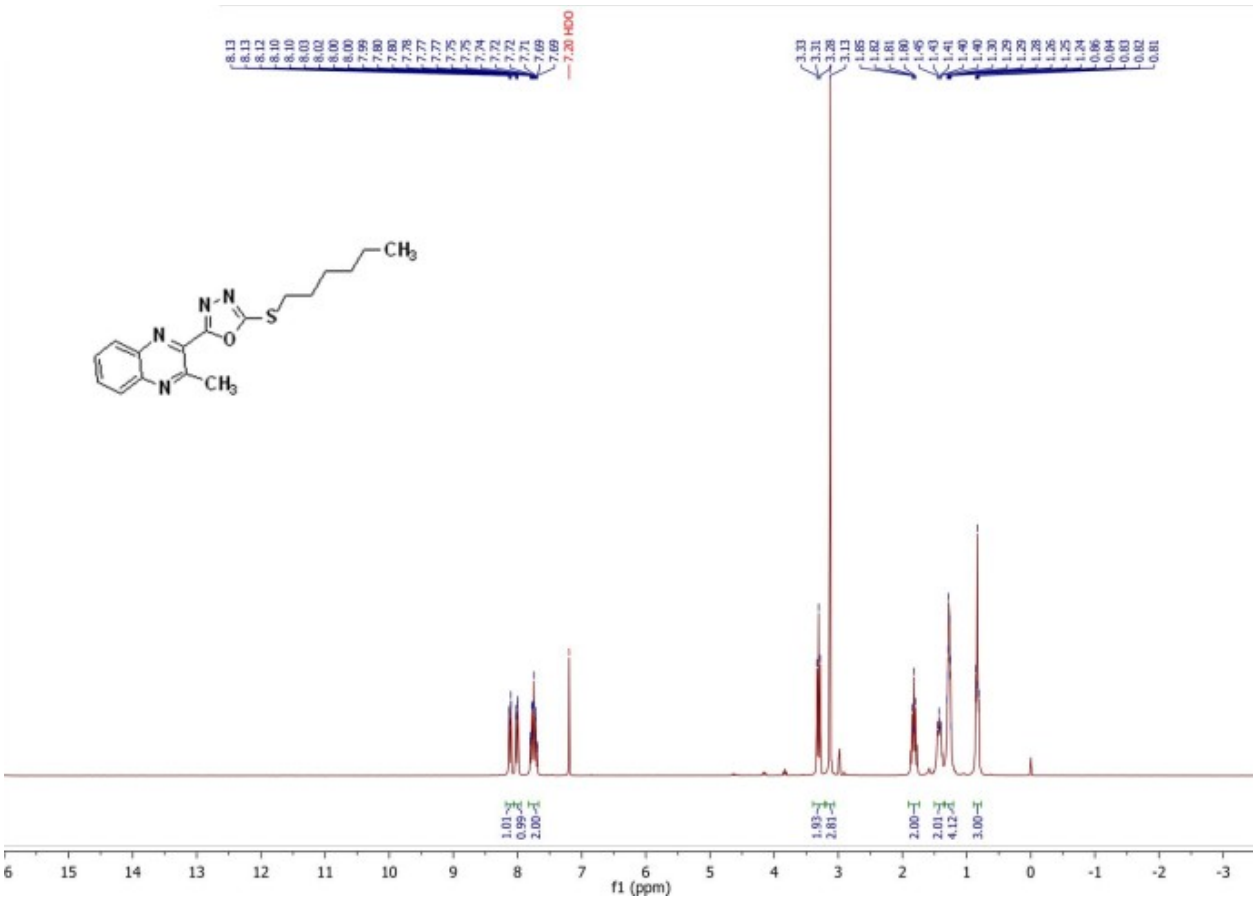

FIGURE S27 ^{1}H NMR (300 MHz, $CDCl_3$) of 2-(hexylthio)-5-(3-methylquinoxalin-2-yl)-1,3,4-oxadiazole (**5c**)

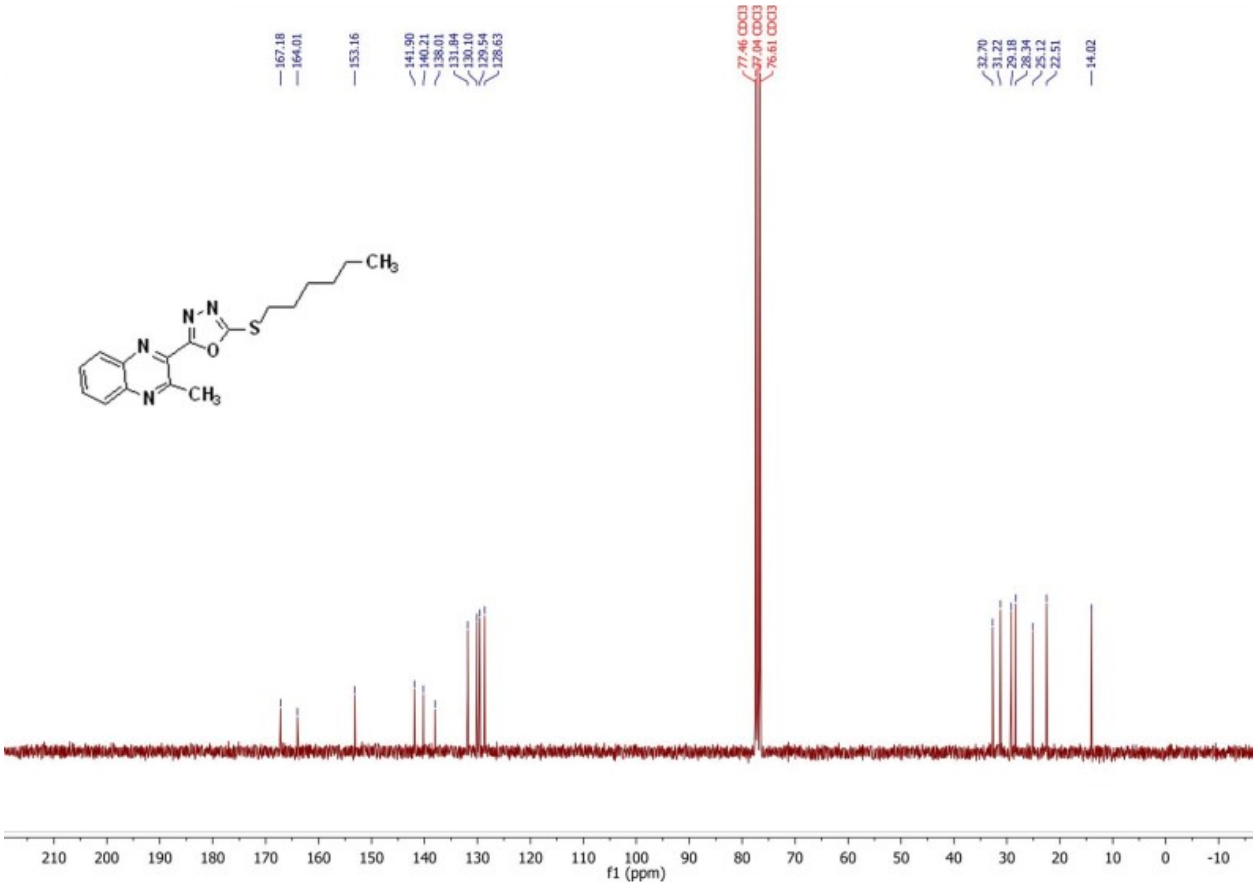

FIGURE S28 ^{13}C NMR (75 MHz, $CDCl_3$) of 2-(hexylthio)-5-(3-methylquinoxalin-2-yl)-1,3,4-oxadiazole (**5c**)

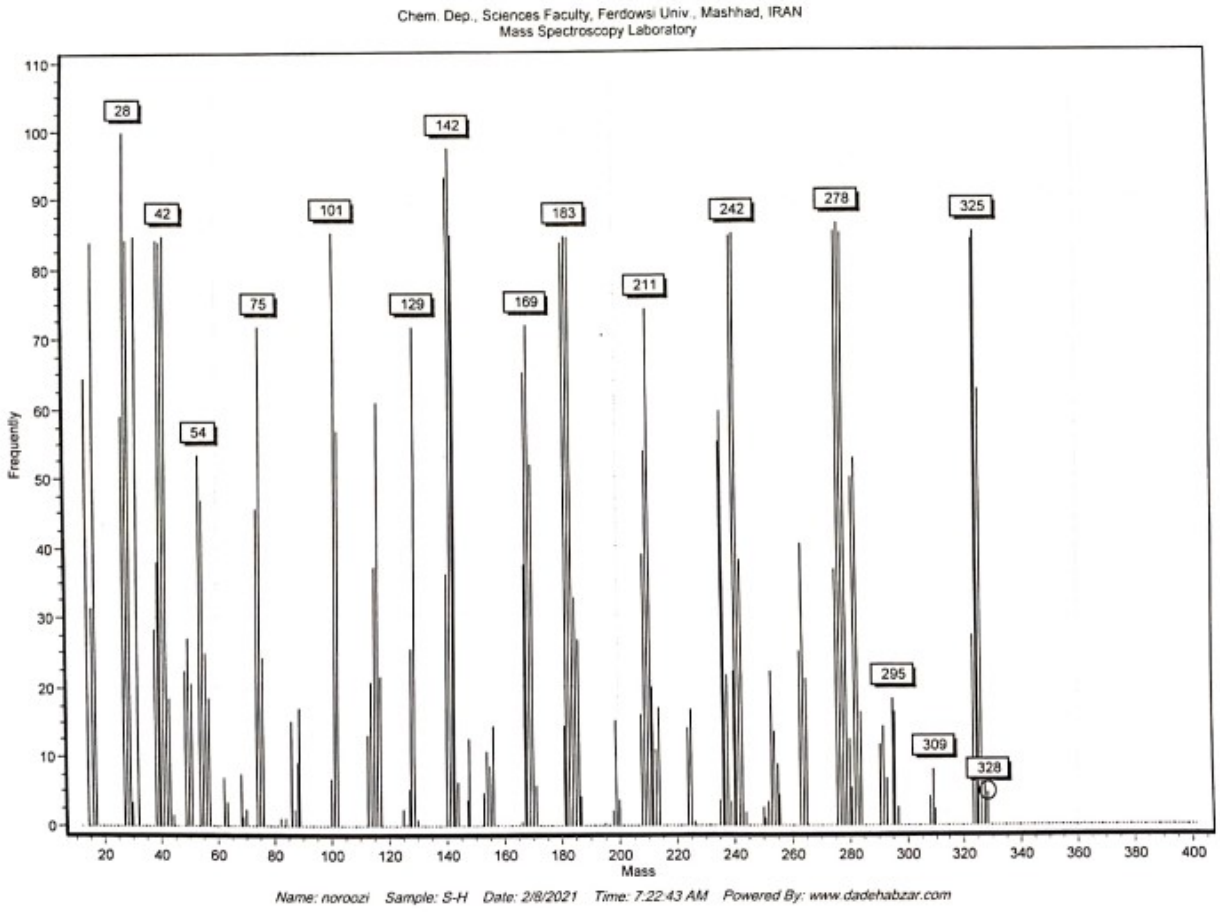

FIGURE S29 Mass spectrum of 2-(hexylthio)-5-(3-methylquinoxalin-2-yl)-1,3,4-oxadiazole (**5c**)

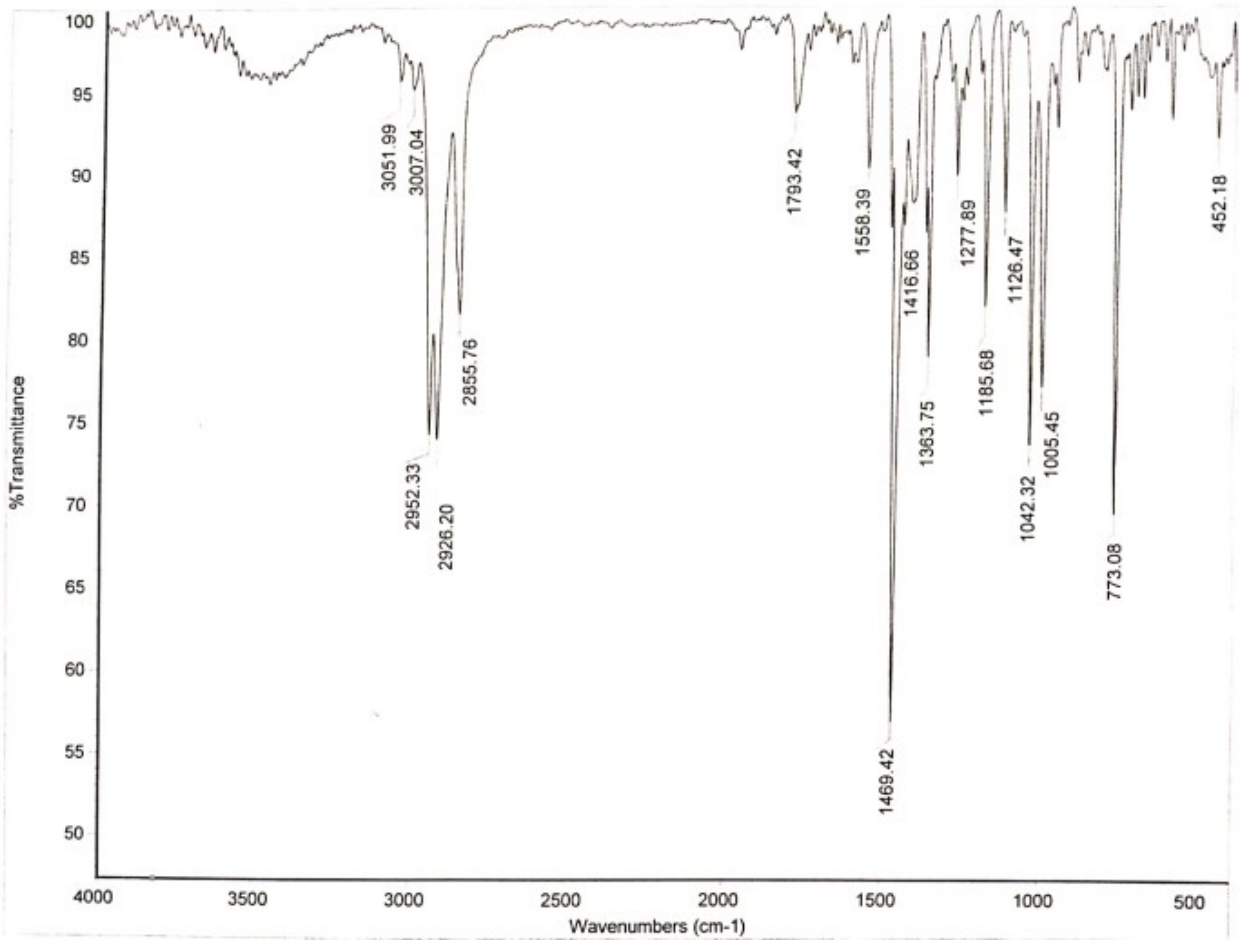

FIGURE S30 FT-IR (KBr) of 2-(hexylthio)-5-(3-methylquinoxalin-2-yl)-1,3,4-oxadiazole (**5c**)

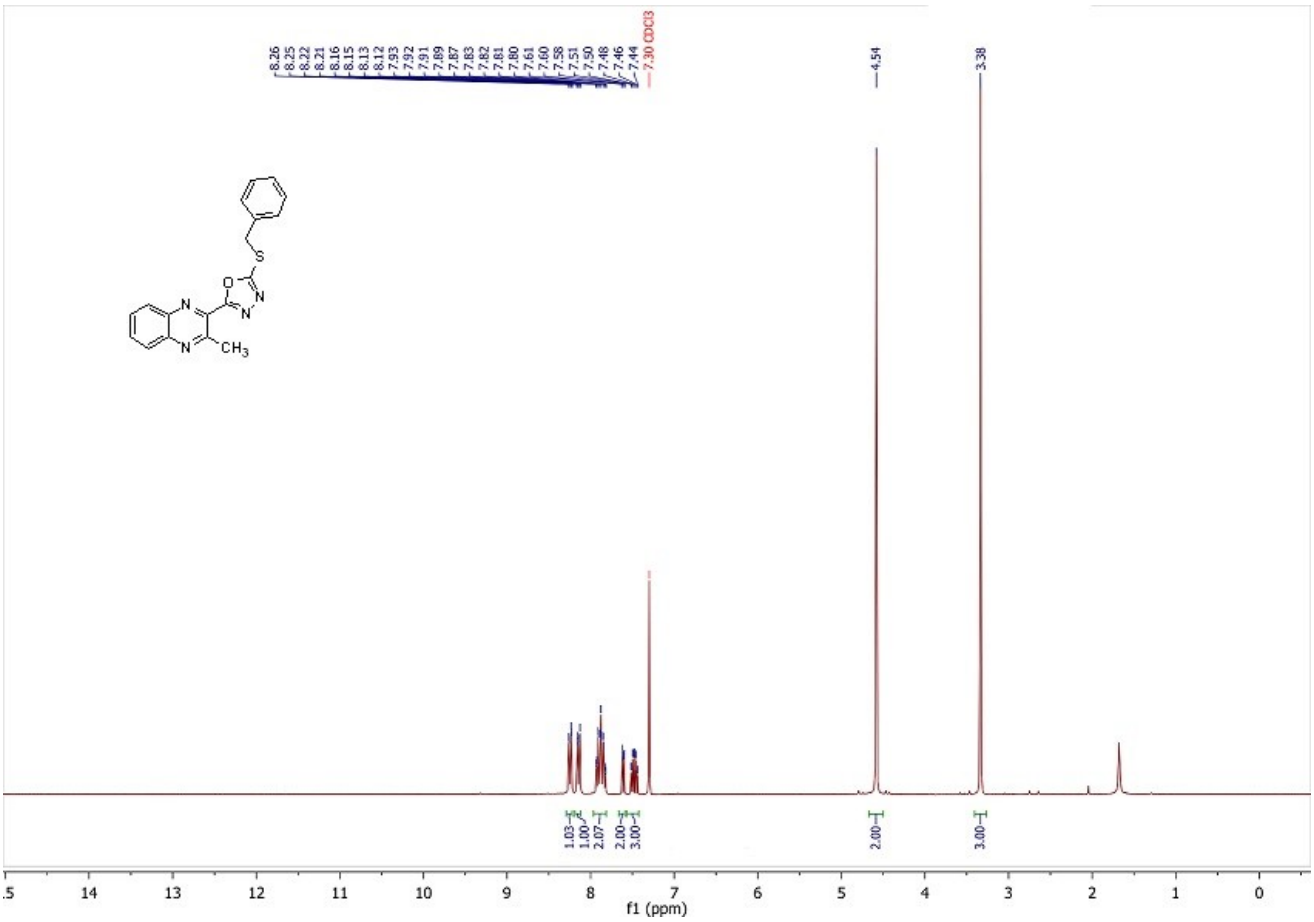

FIGURE S31 ^{1}H NMR (300 MHz, DMSO-d_6) of 2-(Benzylthio)-5-(3-methylquinoxalin-2-yl)-1,3,4-oxadiazole (**5d**)

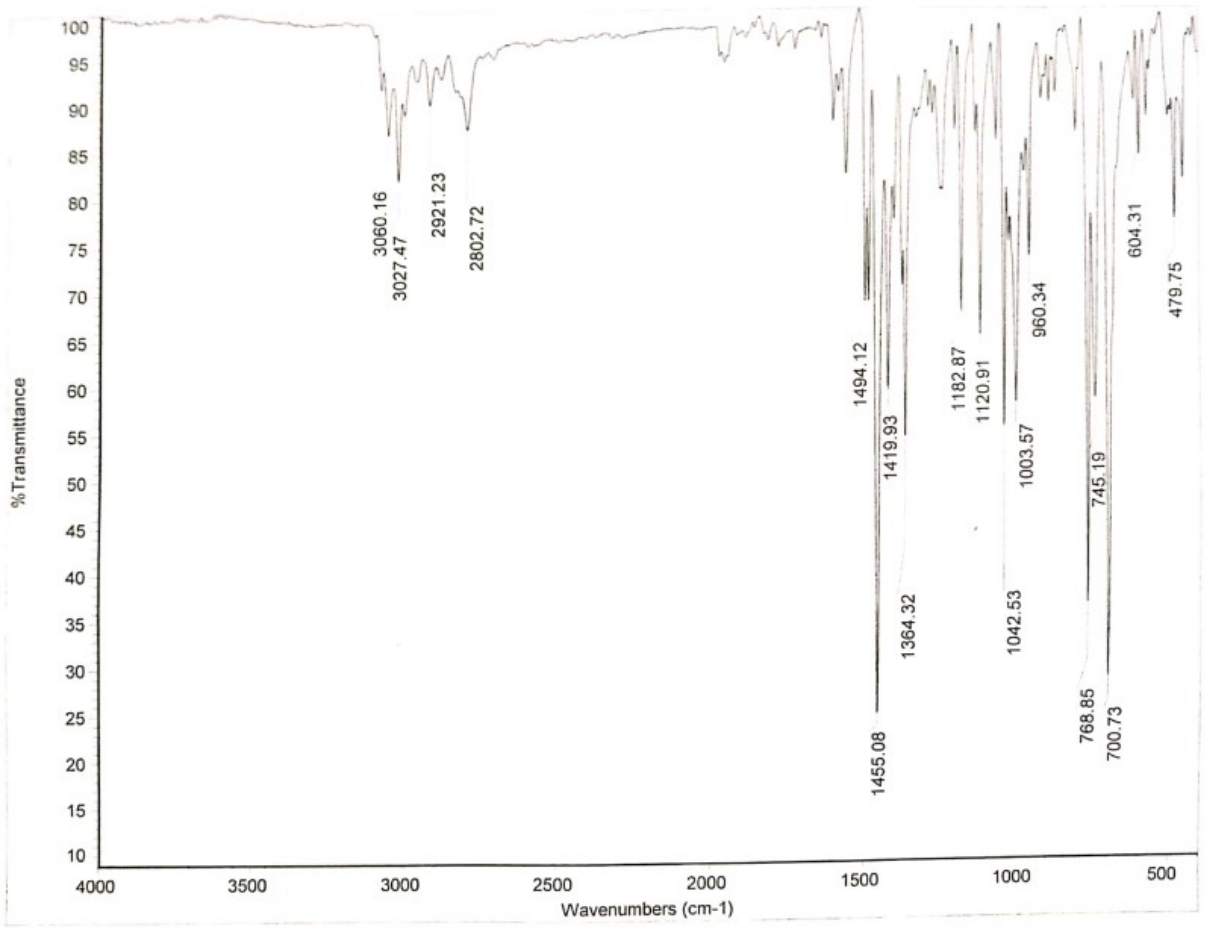

FIGURE S32 FT-IR (KBr) of 2-(Benzylthio)-5-(3-methylquinoxalin-2-yl)-1,3,4-oxadiazole (**5d**)

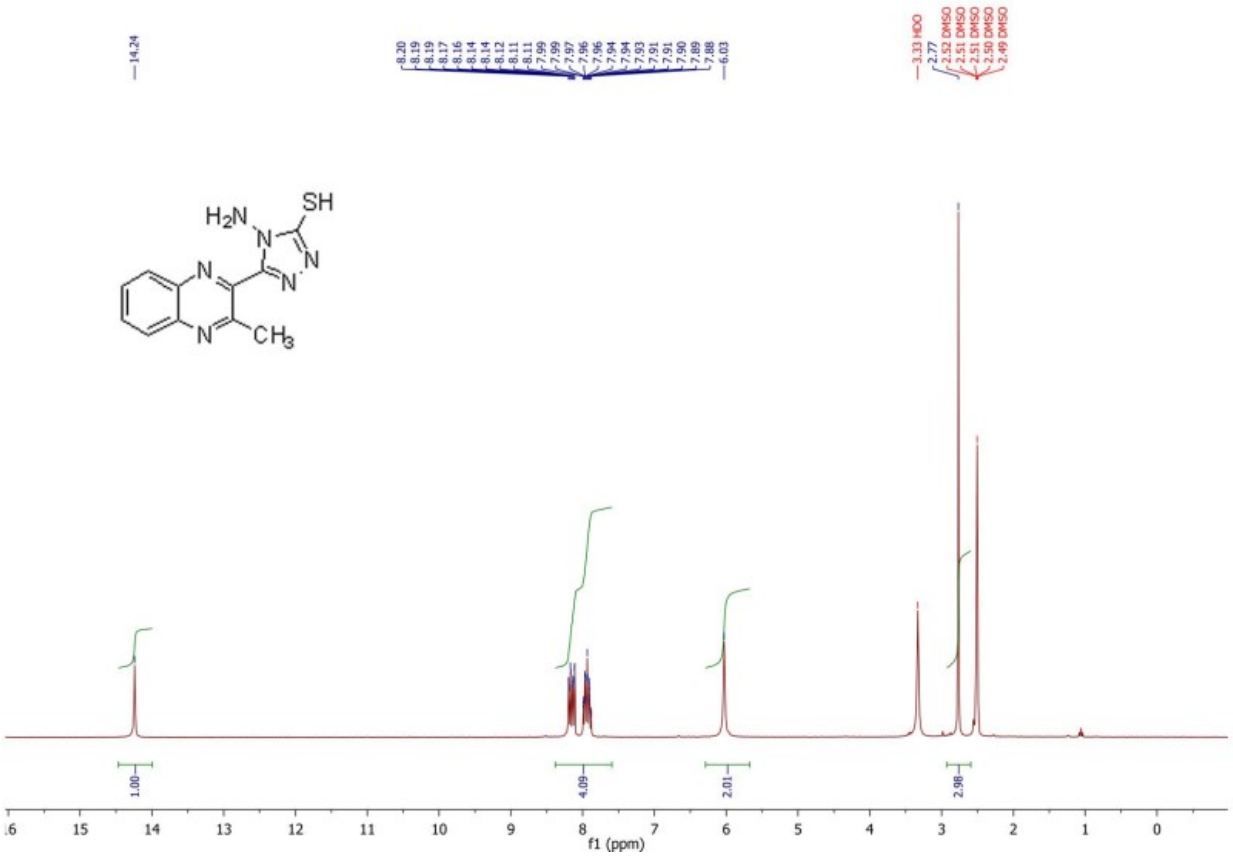

FIGURE S33 ^{1}H NMR (300 MHz, DMSO-d_6) of 4-amino-5-(3-methylquinoxalin-2-yl)-4H-1,2,4-triazole-3-thiol (**6**)

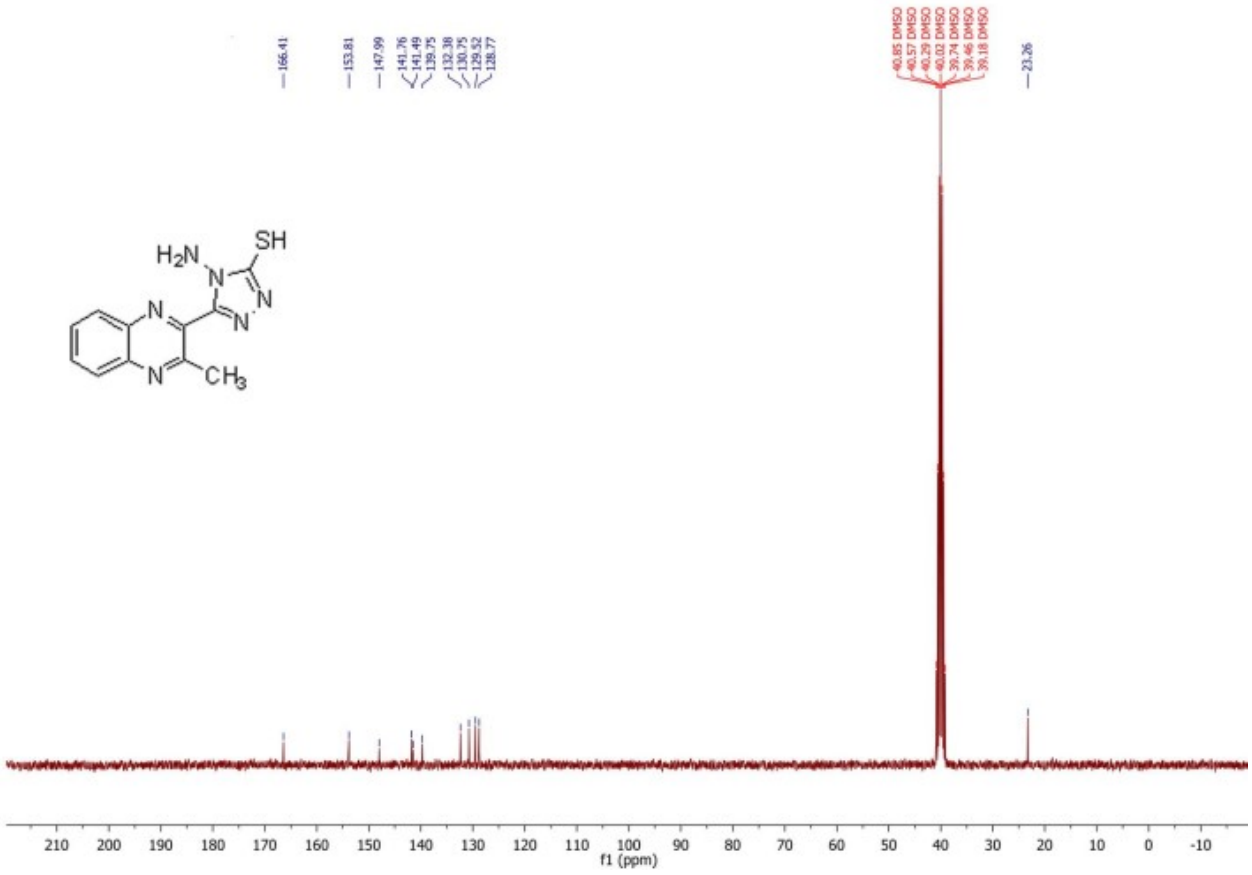

FIGURE S34 ^{1}H NMR (300 MHz, DMSO-d_6) of 4-amino-5-(3-methylquinoxalin-2-yl)-4H-1,2,4-triazole-3-thiol (**6**)

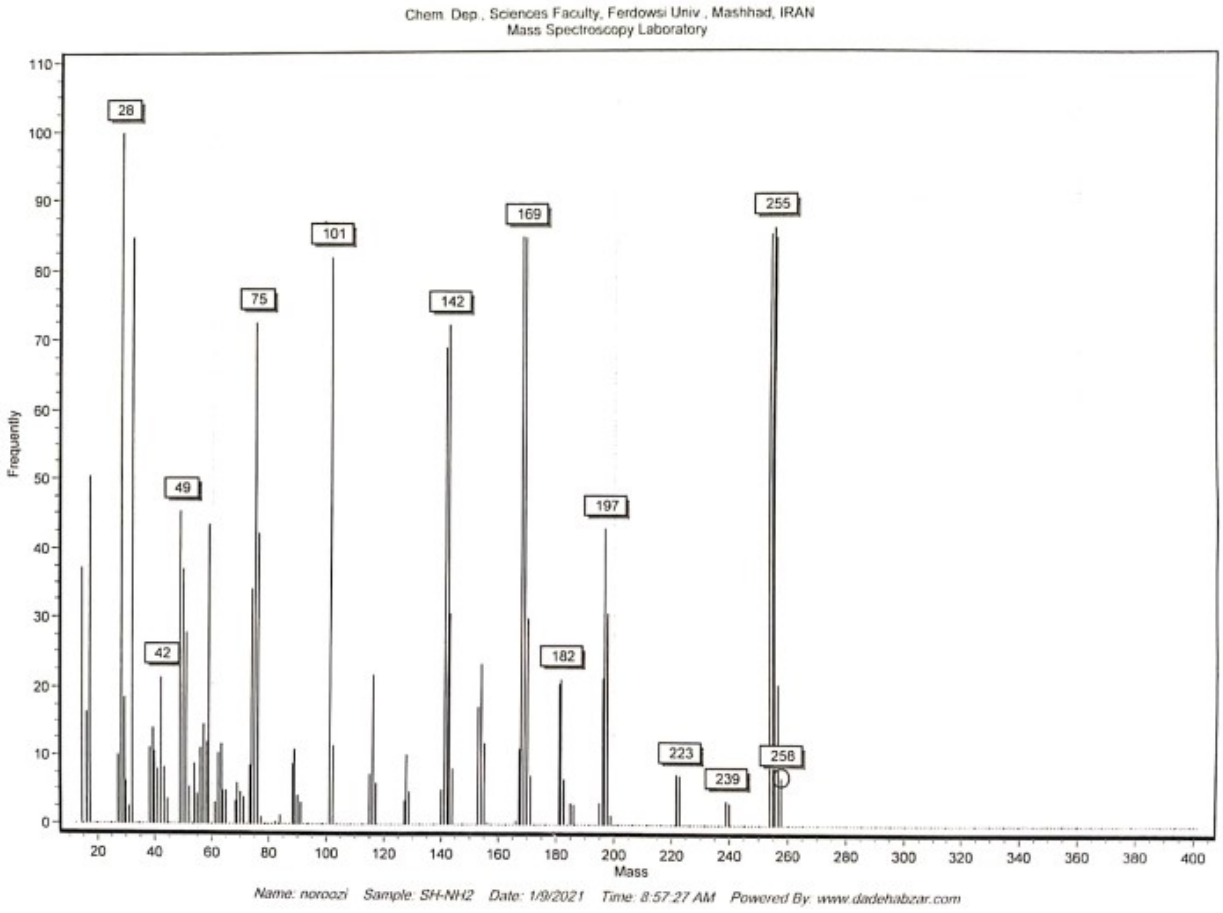

FIGURE S35 Mass spectrum of 4-amino-5-(3-methylquinoxalin-2-yl)-4H-1,2,4-triazole-3-thiol (**6**)

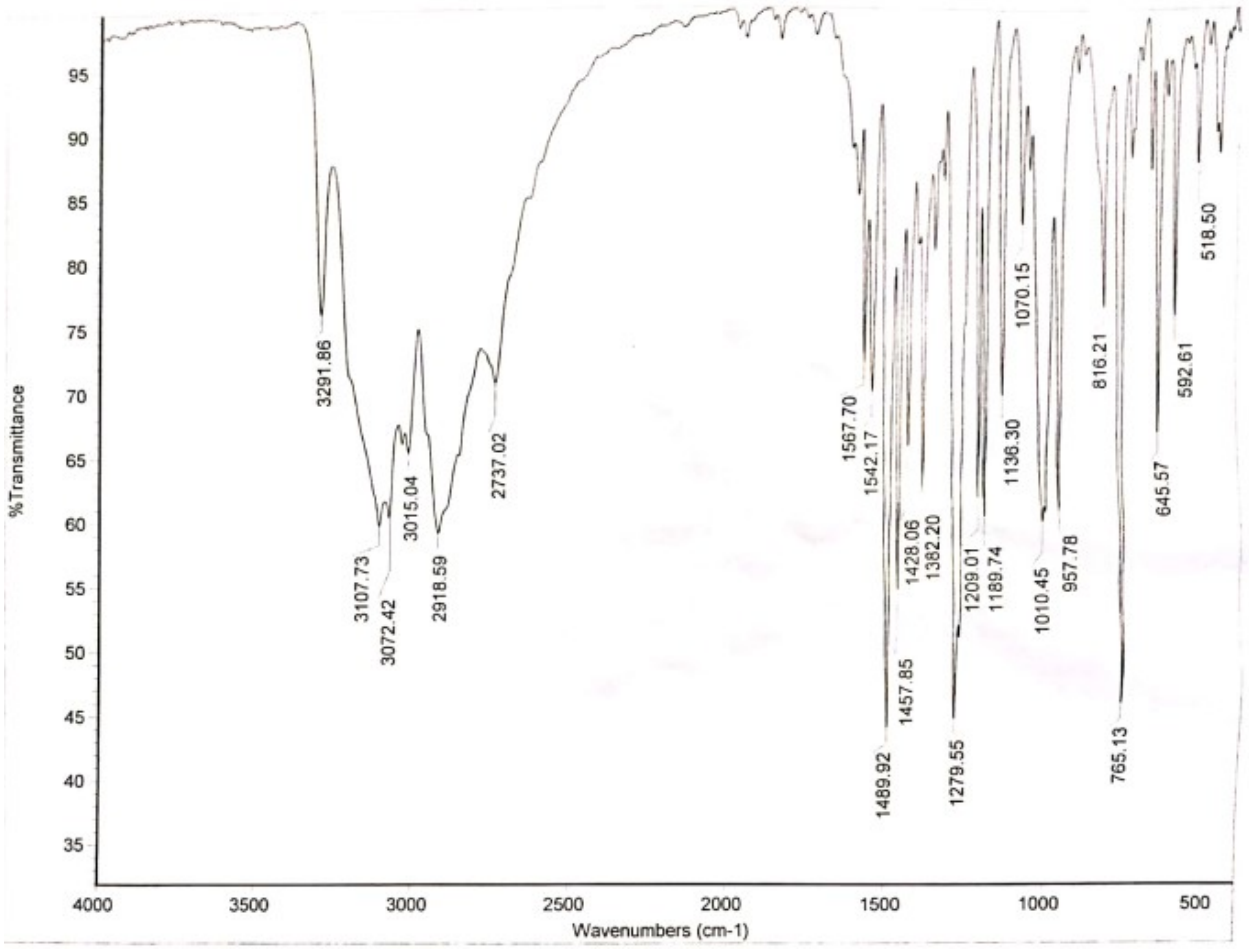

FIGURE S36 FT-IR (KBr) of 4-amino-5-(3-methylquinoxalin-2-yl)-4H-1,2,4-triazole-3-thiol (**6**)